Correlation of Ca-41 and C-14 in activated heavy concrete

Master Thesis

Faculty of Mathematics and Natural Science

University of Cologne

Master of Science in Chemistry

Submitted by

Marco Michel

Supervisor:

PD Dr. Erik Strub

Cologne, May 2023

Eidesstattliche Erklärung

Hiermit versichere ich, Marco Michel, an Eides statt, dass ich die vorliegende Arbeit mit dem Thema

"Correlation of Ca-41 and C-14 in activated heavy concrete"

selbstständig und ohne die Benutzung anderer als der angegebenen Hilfsmittel angefertigt habe.

Alle Stellen, die wörtlich oder sinngemäß aus veröffentlichten oder nicht veröffentlichten Schriften entnommen wurden, sind als solche kenntlich gemacht.

Die Arbeit ist in gleicher oder ähnlicher Form oder auszugsweise im Rahmen einer anderen Prüfung noch nicht vorgelegt worden.

Ich versichere, dass die eingereichte elektronische Fassung der eingereichten Druckfassung vollständig entspricht.

Köln, 08.05.2023
_____
(Ort, Datum)

M. Michel
_____
(Unterschrift)

Table of Contents

List of Figures

List of Tables

Danksagung

Abstract

In this work, the focus was on investigating a possible correlation between the activities of the radionuclides ^{41}Ca and ^{14}C in irradiated reactor concrete. Both nuclides are formed by activation by thermal neutrons from the respective stable nuclides ^{40}Ca (^{40}Ca(n,γ)^{41}Ca) and ^{14}N (^{14}N(n,p)^{14}C). Due to their relevance of nuclear waste disposal and decommissioning of nuclear facilities, ^{41}Ca and ^{14}C become possible key nuclides to characterise irradiated concrete. Both nuclides are challenging to be quantified using radiometric methods but both are commonly measured by accelerator mass spectrometry (AMS). The ^{14}C might often be measured without chemical pretreatment, so the aim of this work was to check whether the measurement of ^{14}C in reactor concrete can be used as a proxy of ^{41}Ca in the material. This would enable for an easier and faster characterisation of irradiated reactor concrete, as the chemical preparation of concrete samples for ^{41}Ca by AMS could be avoided.

For this purpose, barite-enriched heavy concrete was irradiated with thermal neutrons under defined conditions, was examined for Ca and Ba and the concentration of ^{41}Ca and ^{14}C was investigated using AMS. AMS it and examines the atomic number ratio ^{41}Ca/^{40}Ca and ^{14}C/^{12}C with a very low limit of detection.

^{14}C and ^{41}Ca measurements were performed at the CologneAMS of the University of Cologne. For comparison, additional ^{41}Ca measurements were performed at the VERA facility of the University of Vienna using laser-assisted AMS (ILIAMS). The values from both AMS facilities compared with each other as well as with the ^{14}C concentrations. Further, the used concrete was also characterised from nitrogen, as nitrogen is the main source for ^{14}C in concrete.

The comparison of the data showed that a simple correlation of ^{14}C and ^{41}Ca in irradiated concrete is very challenging, at least for lower neutron expositions. While ILIAMS might provide an easier way for the direct determination of ^{41}Ca with a simplified procedure (with respect to conventional AMS), still at least some chemical treatment is necessary in case of heavy concrete samples.

1. Introduction

Nuclear power is currently phased out in Germany. The nuclear power plants (NPPs) in Germany have been gradually taken off the grid over the past 20 years, the last operations being ceased in spring 2023. After the final shutdown, the reactors have to be decommissioned and gradually dismantled. This process generates large amounts of contaminated and/or activated waste, especially from the primary circuit. However, large parts of the control area and the external structure of a facility can be deposited conventionally after appropriate clearance measurements. The concrete material of the biological shield, which encloses the primary circuit in the reactor, is of particular interest, especially concerning the large amount of material, about 10^9 kg. The inner part must be stored as radioactive waste. In contrast, the outer part can be disposed of conventionally if it can be proven that the material is below the relevant clearance values given in the "Radiation Protection Ordinance (Strahlenschutzverordnung)".[1]

It is crucial to know the radionuclide content inside the concrete, as this allows an estimation of their activity to maximize the amount that can be deposited conventionally. The most frequently occurring radionuclides in the biological shield of a NPP as well as their half-life and type of decay are shown in **Table 1**.[2]

Table 1: Most frequent radionuclides in the biological shield with their respective halt-life, type of decay and decay energy [keV].[3]

Radionuclide	Half-life [a]	Type of decay	Energy [MeV]
^{3}H	12.33	β^-	0.185
^{14}C	$5.73 \cdot 10^3$	β^-	0.156
^{41}Ca	$1.02 \cdot 10^5$	ϵc	0.421
^{55}Fe	2.74	ϵc	0.231
^{60}Co	5.27	β^-, γ	2.823
^{63}Ni	100.10	β^-	0.700
^{133}Ba	10.51	ϵc, γ	0.518
^{152}Eu	13.54	β^-, ϵc, γ	1.820 (β^-), 1.874 (ϵc)

Some of these radionuclides, such as ^{3}H, ^{14}C, ^{41}Ca and ^{55}Fe, are difficult to measure using radiometric quantification (like semiconductor γ-detectors or liquid scintillation counting (LSC)). To determine the activities of the difficult-to-measure radionuclides for the release

process, typically so-called key nuclides that are easier to measure are used, e.g. ^{60}Co. On this base, so-called nuclide vectors are established, i.e. fixed ratios of different radionuclides in a specific material or in specific part of a NPP. With the nuclide vectors, the total activity and that of the individual nuclides during the clearance measurements in calculated on the base of the key nuclides only. ^{60}Co, ^{137}Cs and ^{152}Eu are examples used as key nuclides. The activity of the nuclide vector $A_V = \begin{bmatrix} A_1 \\ A_2 \\ A_3 \end{bmatrix}$ results from the determined activity $A_S = \begin{bmatrix} A_1 \\ x \cdot A_1 \\ y \cdot A_1 \end{bmatrix}$ with x and y as the respective contributions of the to be determined activities A_2 and A_3 to the measured activity of A_1 and by multiplying an extrapolation factor f_{SV}, see **formula 1**.

$$A_V = A_S * f_{SV} \tag{1}$$

The extrapolation factor is determined by examining a representative sample as the ratio of the activity of the radionuclide to be determined to the activity of the associated key nuclide.

In the case of a biological shield, establishing a nuclide vector including an easy-to-measure nuclide is challenging: While irradiated concrete will contain radionuclides that can be easily measured by γ-detectors (like ^{60}Co, ^{137}Cs and ^{152}Eu), all these nuclides are formed by the activation of trace elements (Co, Cs, Eu). Therefore, their distribution might be inhomogeneous in the material. On the other hand, the activation of main components of the concrete, like Ca, Ba or Cl, or minor components like C (typically in the % level) or N (~100 ppm) are favoured for measurement.

The search for possibilities for further key nuclides and other methods to establish radiological characterization will play a crucial role in the future. With their very low detection limit, LSC and AMS are suitable as additional methods for investigating potential new key nuclides.[4,5]

A major advantage of the AMS is the non-radiometric measurement of the radionuclides. Therefore, it is possible to measure nuclides with a long half-lifes since it is not necessary to wait for individual decays, but to measure the atomic ratio between a radionuclide and a stable isotope for quantification. With the LSC method, very small detection limits can also be achieved, but the measurement of a continuous beta spectrum requires complex processing in order to separate interfering beta emitters. Beta emitters from the natural decay chains must also be considered. Such a complex chemical treatment is not necessary for the AMS since other radionuclides do not interfere with the measurement. Nevertheless, a rough concentration of the sample is necessary and for the measurement the stable isobars must be

suppressed and previously separated as far as possible. Therefore, a key nuclide that can be measured with these methods without chemical processing would be suitable. This could help in future release processes to save more material for disposal and to make it more variable through new methods.

2. State of Knowledge

2.1   AMS in decommissioning of nuclear facilities

Analysis of ^{41}Ca in reactor graphite has already been performed at the CologneAMS, see the work of R. Spanier, R, Margreiter and M. Michel.[5–7]

For this purpose, the chemical procedure for the separation of Ca from soil samples had been adapted. It was shown that the procedure (which originally was developed for LSC measurements, see Lehto and Hou *et al.*)[8,9] could be simplified. While it is still necessary to concentrate Ca in the sample, the separation has not to be quantitative in a strict sense, because e.g. the homologue ^{133}Ba does only interfere in LSC measurements, but not in AMS:

Also, a yield control, e.g. by radioactive tracers, is not required as AMS measures the ^{41}Ca/^{40}Ca ratio, which does not depend on the yield as both nuclides are isotopes.

However, preparation of ^{41}Ca samples for is still more elaborate then for ^{14}C. Also, the installation of an elemental analyser (EA) and a gas injection system (GIS) at CologneAMS [10] allows for an AMS measurement of combustion gases which enables for ^{14}C AMS without prior chemical separation, at least when the concentration of ^{14}C is higher than the natural background. This has recently been proven for the application of ^{14}C measurements in reactor graphite.[10,11]

Like ^{41}Ca, ^{14}C has already been analysed from concrete samples at the CologneAMS. For this purpose, concrete samples were taken from of a so-called nuclear 'small facility' and investigated whether an increased activity of certain radionuclides, ^{14}C, ^{36}Cl and $^{239/240}$Pu, could be measured after the duration of operation as a result of working with radioactive substances. Due to the very sensitive detection limit of the comparatively rough chemical processing of the samples, AMS was the method of choice.[12] Both ^{14}C and ^{41}Ca are produced by neutron irradiation of reactor concrete, hence ^{14}C might be used as a proxy for ^{41}Ca in reactor concrete, further simplifying chemical pre-treatments for AMS.[5]

2.2 CologneAMS

CologneAMS is an accelerator facility in the Institute for Nuclear Physics at the University of Cologne and has been in routine operation since 2011.[13] A 6 MV tandem accelerator is installed in the AMS facility. This makes it possible to study a wide range of radionuclides, including many of the cosmogenic nuclides, such as ^{10}Be, ^{14}C ^{26}Al, ^{36}Cl and ^{41}Ca and also the measurements of Pu isotopes is possible. [12,14,15] A scheme for the structure of the CologneAMS is shown in **Figure 1**, more detailed descriptions in **Chapter 4.1.4.1.**
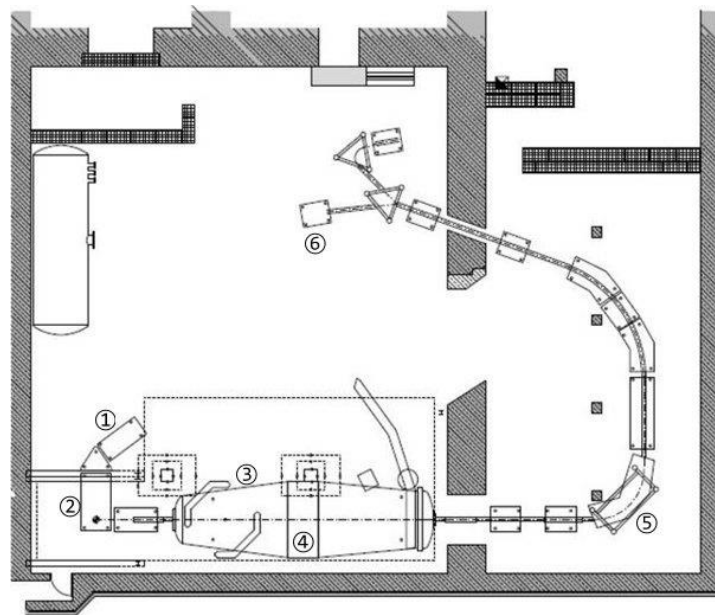
Figure 1: Schematic structure of the CologneAMS in the Institute for Nuclear Physics at the University of Cologne. (Modified to [13])

2.3 Vienna Environmental Research Accelerator (VERA)

VERA is an accelerator facility built in the Faculty of Physics – Isotope Physics of the University of Vienna and optimized for AMS. It went into operation in 1996 and has been expanded and modified several times during this time in order to examine a broad spectrum of radioisotopes in the chart of nuclides, see Golser *et al.* [16]

The unique feature of this system is the so-called Ion Laser InterAction Mass Spectrometry (ILIAMS) attached to the AMS, as shown in **Figure 2**. This highly efficient filter method suppresses isobaric nuclides from the ion beam through selective laser neutralization of cooled anions. Different electron affinities of the ion of interest and interfering isobars are used to de-ionise selectively the isobar, as described in the work of Martschini *et al.* [17] and Schiffer *et al.*.[18] This makes it possible to make new trace isotopes in typical environmental

concentrations accessible through AMS measurements and to further reduce the detection limit for nuclides already detected, such as [26]Al, [36]Cl and [182]Hf.[19–21]
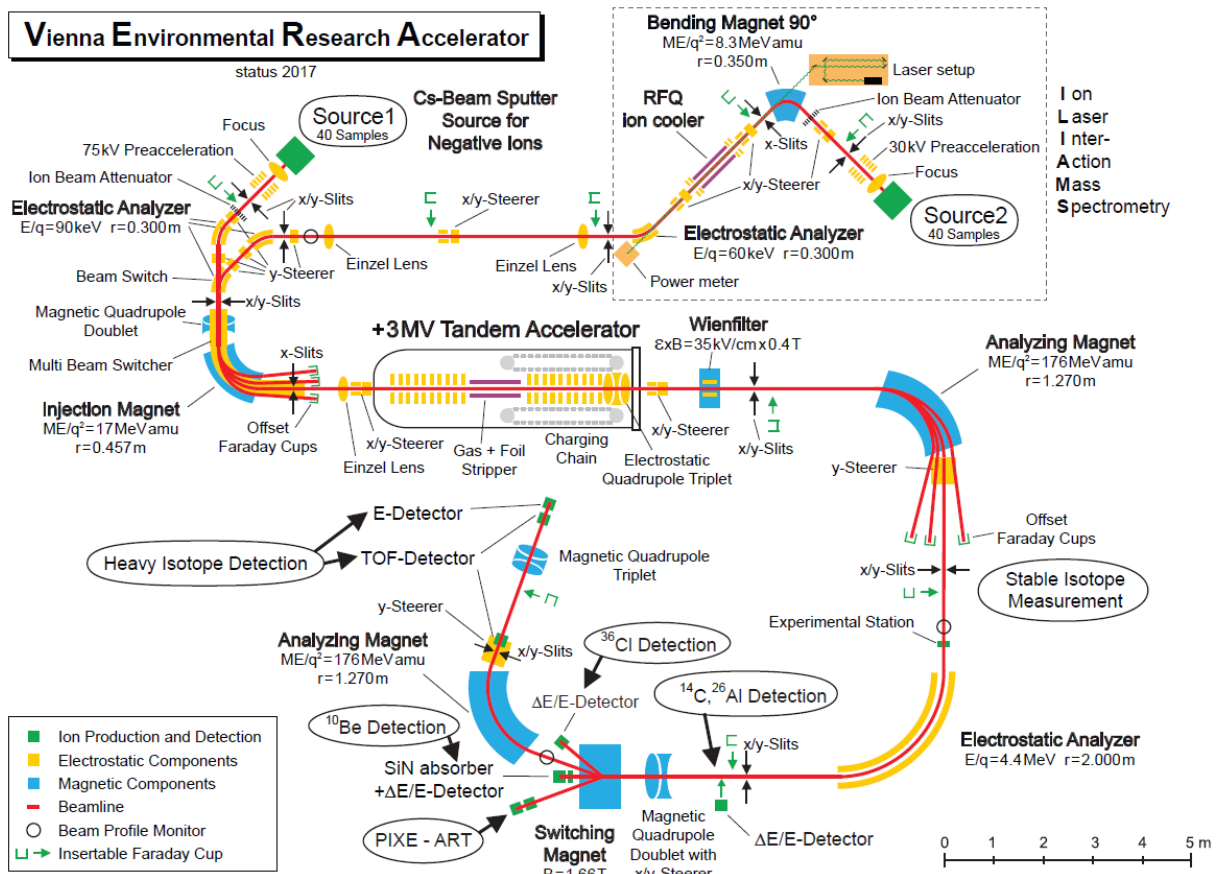
Figure 2: Scheme of the AMS at VERA with the ILIAMS system. Received from Golser et al. [16]

2.4   AMS of [41]Ca

2.4.1   Origin and Applications of [41]Ca

The radionuclide [41]Ca is formed from the stable isotope [40]Ca by a (n,γ) nuclear reaction by thermal neutrons with a neutron capture cross-section of 0.40 ±0.04 barn, see Cranston *et al.*[22]. The half-life is $1.04 \cdot 10^4$ a, see Nishiizumi *et al.*[23]. It decays to the stable [41]K by electron capture, emitting X-rays and low-energy (0.3 - 3.6 keV) Auger electrons.[24]

Due to its long half-life, [41]Ca is used for exposure dating and for determining the age of meteorites using AMS.[25] In medicine, radionuclides are used as a tracer to study metabolic processes in the human skeleton, see Freeman *et al.*[26] and to study cancer in human bones, see Shen *et al.* also using AMS.[27]

In addition to these applications, AMS can be used to characterize the ^{41}Ca concentration in building materials of nuclear facilities due to the increasingly important task of decommissioning.[28] This can help in the process of dismantling to separate activated parts from simple rubble. Determining the ^{41}Ca content in activated concrete is important due to its high biodiversity, Ca could be incorporated into organic structures and thus easily get into the human body, where it would preferentially accumulate in the bones. Therefore, the clearance levels for unrestricted release of ^{41}Ca is ~100 Bq. This is on a higher level as ^{14}C, where the limit is set at ~1 Bq. Compared to tritium (^{3}H), which has an clearance level of ~100 Bq due to its short biological half-life, the release values of ^{41}Ca and ^{14}C are relatively low. [1]

The exemption limits of both ^{41}Ca and ^{14}C are at ~10^6 Bq/g. ^{3}H in comparison has a exemption limit of ~10^8 Bq/g.[1]

An overview of ^{41}Ca in the nuclide chart with the surrounding nuclides is shown in **Figure 3**.

Figure 3: ^{41}Ca in the nuclide chart with the surrounding nuclides.[3]

2.4.2 ^{41}Ca measurements of irradiated samples (AMS, LSC)

The activity of ^{41}Ca is routinely determined using liquid scintillation counting (LSC) and accelerator mass spectrometry (AMS). LSC is challenging, as ^{41}Ca is a pure electron capture nuclide which must be quantified measuring the 3 keV Auger electrons. On the other hand AMS measurement method for measuring ^{41}Ca is well established and is routinely carried out in many facilities worldwide.[5,29–31]

The ^{41}Ca/^{40}Ca ratio is determined from the used sample and, in the case of the CologneAMS, the detection limit is as low as 10^{-15}, determined by R. Spanier in his dissertation.[5] One difficulty is the preparation of the samples for measurement. Depending on whether the ^{41}Ca is measured using LSC or AMS, the focus of the chemical treatment varies. In the decay-based measurement at the LSC, separating all competing beta emitters that may be

superimposed on the [41]Ca peak is essential. Therefore, a complex and exact separation is required, described in the work of Hou.[9]

In addition to the complex preparation process, the measurement of [41]Ca only has a counting efficiency of 25 % due to the low energies of the Auger electrons released. Compared to other examined radionuclides, this value is relatively low [9] and adds to the uncertainty budget.

However, less complex preparation is necessary for the measurement with AMS since the type of decay is irrelevant due to the mass-based measurement and for the preparation of the samples, special attention must be paid to the separation of isobaric nuclides; in the case of [41]Ca, this is only the stable [41]K.[6]

In recent years, separation procedures for the preparation of Ca from sediments and soils for LSC measurements have been developed, see the work of Hou.[9] These were modified in recent works to allow the purification of Ca from concrete for AMS measurements; see the scheme in **Figure 4**.[6,9]
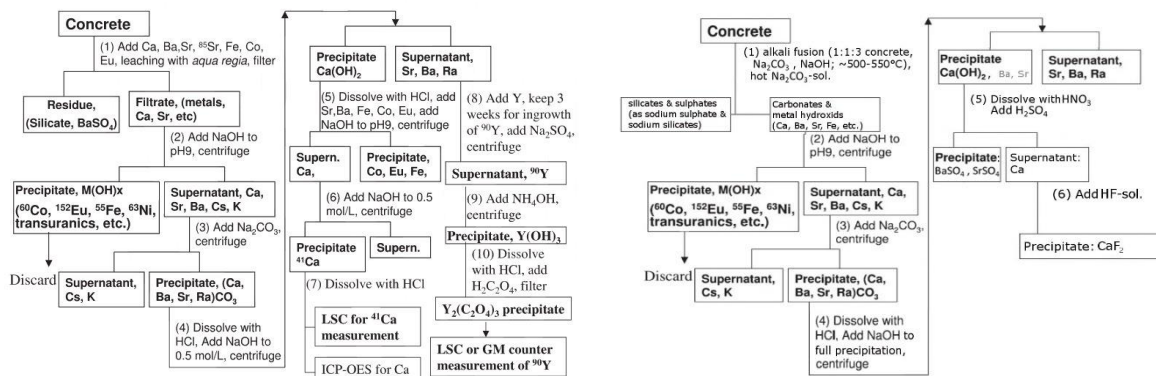
Figure 4: Comparison of the schemes of the calcium separation procedure from concrete samples developed by Hou for LSC measurements (*left*) and R. Margreiter for AMS measurements (*right*).[9,6]

The scheme developed by Hou in **Figure 4** has been simplified significantly by R. Margreiter. In addition, after successfully modifying the separation, the quantitative yield of Ca was also examined and determined.[7,32]

To carry out the measurement more precisely and to use it for possible investigations into the clearance measurement of material from the biological shield, [41]Ca was investigated as a possible reference nuclide for AMS measurements.[5] For this purpose, test samples of heavy concrete with a composition comparable to the material of the biological shield were activated with neutrons. Then the composition of the formed radionuclides ^{3}H, ^{14}C and [41]Ca was successfully examined.[5]

2.4.3   Calculation of expected ^{41}Ca activities

The amount of produced ^{41}Ca and the resulting ratios of ^{40}Ca/^{41}Ca were calculated based on the amount of ^{40}Ca inside the used barite concrete; see **Chapter 5.1**. The production process of a nuclide N_B originating from a number of particles N_A, including the decay is described in the general **equation 2**.

$$\frac{dN_B}{dt} = \sigma * \phi * N_A - \lambda * N_B \tag{2}$$

With: $\lambda = \frac{\ln(2)}{T_{1/2}}$

Based on this equation, the activity of the produced nuclide B can be calculated by integrating **equation 3** the equation of the time t.

$$A(t) = \sigma * \phi * N_A * (1 - e^{-\frac{\ln(2)t}{T_{1/2}}}) \tag{3}$$

From **equation 3** can be calculated the number of ^{41}Ca particles and the ^{41}Ca/^{40}Ca ratios. The calculated numbers are based on the given neutron flux ϕ, the amount of ^{40}Ca in 1 g barite concrete N_A, the irradiation time t and the half-life of ^{41}Ca $T_{1/2}$ = 9.94 ±0.15 · 10^4 a, see Jörg *et al.* [33] The thermal neutron capture cross section for ^{40}Ca is σ = 0.40 ±0.04 barn.[22]

In order to match the target concentration of ^{41}Ca as closely as possible to that in the biological shield of a nuclear reactor, the neutron flux distribution inside the reactor pressure vessel and in the biological shield was considered radial to the distance to the reactor core, see **Figure 5**. At the outer regions at about 3.4 m, a neutron flux of ~5.0 · 10^7 N/cm^{2}s with an energy of <0.41 eV, which corresponds to the energy of epithermal neutrons, is to be expected. This corresponds to an annual neutron flux of 1.5 · 10^{15} N/cm^2. Comparing the neutron flux during irradiation at the TRIGA reactor ϕ = 1.7 · 10^{12} N/cm^{2}s, a similarly high neutron dose is already reached after an irradiation time of around 1,000 s.

With a neutron flux of 1.5 · 10^{15} N/cm^2 per year, a ^{41}Ca activity of 1.41 Bq/g is achieved in the barite concrete. In comparison with the clearance values for the unrestricted release of ^{41}Ca from liquid and solid substances A(^{41}Ca) = 100 Bq/g [1], the value is far below.

A comparison of the calculated ^{41}Ca activities from the neutron fluxes in the biological shield from **Figure 5** with the clearance values for unrestricted release is shown in **Table 2**.

Table 2: Comparison of the calculated A(^{41}Ca) from the determined neutron fluxes from **Figure 3** with the release limits for the unrestricted release of ^{41}Ca from solid and liquid substances.[1]

Distance to reactor core [m]	Neutron flux [N/cm²s]	A(^{41}Ca) per g barite concrete per year [Bq/g]	Clearance value of unrestricted release of ^{41}Ca [Bq/g]
2.35	$2.00 \cdot 10^9$	56.39	100
2.50	$3.50 \cdot 10^9$	98.69	100
2.75	$1.70 \cdot 10^9$	47.93	100
3.00	$6.00 \cdot 10^8$	16.92	100
3.25	$3.10 \cdot 10^8$	8.74	100
3.40	$5.00 \cdot 10^7$	1.41	100
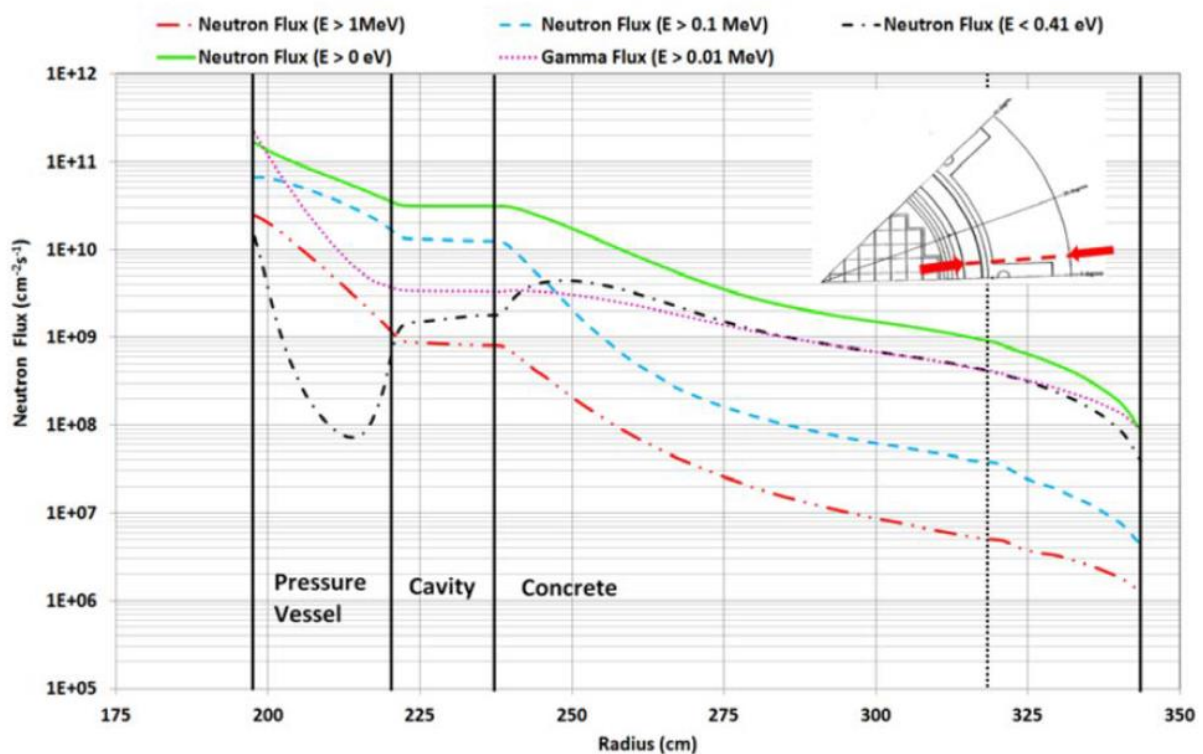
Figure 5: Neutron flux as a function of the radial distance to the reactor.[11]

The values from **Table 2** show that the clearance value of ^{41}Ca in the concrete are not reached after one year of operation. However, when a nuclear reactor is operated over several decades at shorter distances, the limits for unrestricted approval are clearly exceeded in the concrete but there is only a chance of falling below the values at the outer edge of the biological shield. Hence, a certain part of a bioshield can be disposed conventionally, i.e. much cheaper than radioactive disposal.

2.5 AMS of ^{14}C

2.5.1 Radiocarbon dating and origin of ^{14}C

^{14}C is formed naturally in the upper atmosphere by the influence of cosmic rays from ^{14}N through a (n,p) reaction and it is a cosmogenic nuclide.[34]

This results in a relatively constant proportion of ^{14}C of 10^{-10} % of total carbon. It decays to ^{14}N with a half-life of 5730 a [35] by means of beta decay. ^{14}C gets into the organism of living beings through the global carbon cycle, which makes it possible to determine the age of organic material after its death using the radiocarbon method, which is the main application of ^{14}C measurements.

This method was first developed by Willard Frank Libby in 1946.[36] At that time, the determination of the ^{14}C activity was performed by measuring the decay of the nuclide in a counting tube.[36]

Due to the significantly better detection limit, the radiocarbon dating method is usually performed using AMS nowadays. As a result, the ^{14}C/^{12}C ratio can be determined with an accuracy of 10^{-15} and direct detection of the ^{14}C atoms is thus possible. The radionuclide ^{14}C is suitable due to its long half-life of 5730 ± 40 a, described at the work of H. Godwin [35], which means that the age of samples can be determined up to ~57,000 years. An overview of ^{14}C in the nuclide chart with the surrounding nuclides is shown in **Figure 6**.

Figure 6: ^{14}C in the nuclide chart with the surrounding nuclides.[3]

2.5.2 ^{14}C in irradiated samples

Depending on the examined material, two types of reaction for the formation of ^{14}C need to be investigated, the ^{13}C(n,γ)^{14}C with a neutron cross-section of $1.5 \cdot 10^{-3}$ barn [37] and the

^{14}N(n,p)^{14}C reaction with σ = 1.83 ±0.03 barn, see Hanna *et al.* [38] This is important for samples with a significant carbon content, such as irradiated graphite, where the first reaction is the main source of ^{14}C. When examining activated concrete, this formation path is negligible compared to the formation from ^{14}N. The activation equation for the formation of ^{14}C is shown in **formula (2)** in **Chapter 2.4.3**.

An assessment of the distribution of ^{14}C in samples of activated material is given by the work of von Lensa *et al.* [39], where graphite was activated with neutrons and the release of ^{14}C compared to total carbon was shown, see **Figure 7**. The nuclear reaction from which ^{14}C has formed also plays a vital role since the formation of ^{14}C in the graphite pores mainly results from ^{14}N but within the lattice structure from ^{13}C. This suggests that the ^{14}C inside the pores is released more quickly during heating.
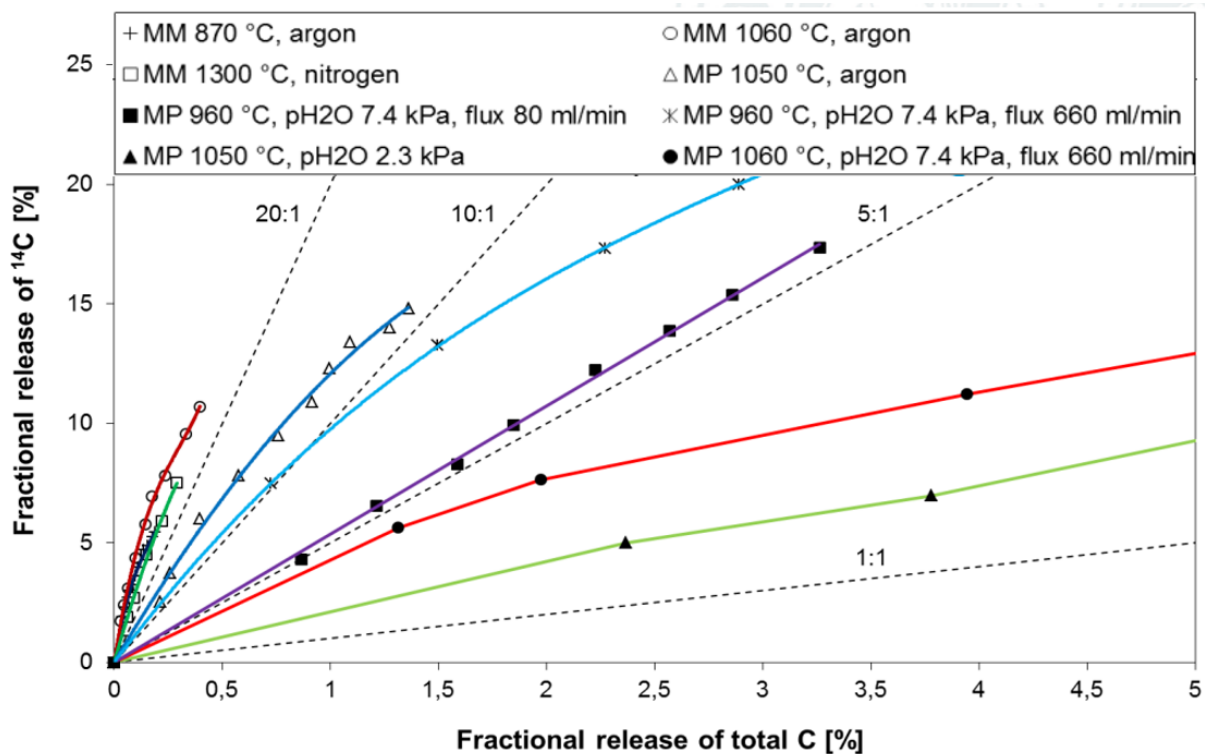
Figure 7: Release of ^{14}C compared to residual carbon in activated graphite at different temperatures, fluxes and crushing types (MM = massive, MP = powdered).[39]

From **Figure 7**, the release of ^{14}C was much faster than the rest of the carbon. This can be characterized by the ratio between ^{14}C and C, where the ratios vary widely with different annealing temperatures, fluxes and degrees of comminution of the sample.

For the investigation of ^{14}C at the CologneAMS, the focus has increasingly been on activated samples from nuclear plants in recent years.[11] As part of this, a gas injection system including an elemental analyser (EA) was connected to the AMS, described in the work of M. Gwozdz [10], as shown in **Figure 8**.

With this system it is possible to analyse the carbon and nitrogen content of organic samples (sediment, soil, concrete). When studying the ^{14}C content of activated samples, it is important to also measure the nitrogen content, since ^{14}C is mainly formed from the nuclear reaction ^{14}N(n,p)^{14}C by thermal neutrons, with $\sigma = 1.83 \pm 0.03$ barn, see Hanna *et al.* [38]

In the master thesis by M. Gwozdz, the gas system mentioned above was also tested with the EA on heavy concrete samples. The nitrogen content of differently crushed heavy concrete (barite concrete) was examined there.[10]
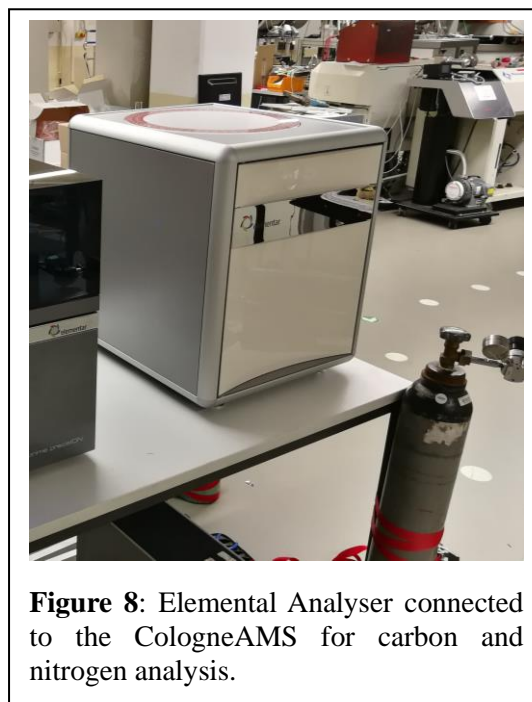
Figure 8: Elemental Analyser connected to the CologneAMS for carbon and nitrogen analysis.

The focus was on the type of comminution (mortar, ball mill) and whether the degree of comminution influences the nitrogen measured. In concrete, nitrogen is mostly present as N_2 in pores and interstices and is incorporated less chemically into the structure. The amount of nitrogen plays a crucial role in future investigations on activated concrete samples since ^{14}C is formed from ^{14}N and is present in the pores, probably mainly as $^{14}CO_2$. This could lead to an uneven distribution of carbon in the EA during combustion. The results of M. Gwozdz showed that no significant change in the nitrogen content could be determined for the different degrees of milling. Still, the deviation in the individual measurements is relatively high, which could lead to the assumption of uneven combustion in the EA.

2.6 ^{41}Ca and ^{14}C as potential key nuclides

Based on the results of the work of R. Spanier [5] on the investigation of ^{41}Ca in barite concrete irradiated at different levels and M. Gwozdz [10] on her investigation of the nitrogen content in concrete, the two radionuclides ^{41}Ca and ^{14}C have the potential as key nuclides to be used for decommissioning.

In his dissertation, R. Spanier investigated the detection limit of the AMS regarding the $^{41}Ca/^{40}Ca$ ratio and examined irradiated barite concrete for the detectability of ^{41}Ca. His investigations also focused on whether ^{41}Ca could be a possible key nuclide. On the one hand, he was able to show by measurements of nominal standards that a detection down to the ratio $R(^{41}Ca/^{40}Ca) = 4.70 \pm 0.79 \cdot 10^{-13}$ is possible.[5] On the other hand, he had barite concrete samples activated with neutrons for irradiation times of 30 - 3000 s and could determine a linear relationship between the measured ^{41}Ca activities. He thus summarized a possible use of ^{41}Ca as a reference nuclide.[5]

When investigating the nitrogen content, M. Gwozdz established a measurement routine at the EA for organic samples in her master thesis. She also increased the sensitivity of the EA for nitrogen and carbon measurements by changing the helium flow, resulting in the concretes nitrogen content being calculated and measured (53.93 ± 10.41 ppm). By calibrating the system using standards, it is possible to measure a series of measurements of nitrogen and carbon with little uncertainty, as described in her thesis. [10]

This opens the possibility of using ^{14}C as proxy for ^{41}Ca. One advantage would be that ^{14}C is easier to measure than ^{41}Ca due to the low level of effort involved in measuring and chemical treatment, and on the other hand that, due to their sufficiently long half-lives and good concentrations in the concrete, these could also be used well in the context of dismantling and decommissioning.

3. The motivation for this work

Based on the thesis of the possible use of ^{14}C and ^{41}Ca as key nuclides, the correlation of the activity of said radionuclides to each other is to be examined within the scope of this work. For this purpose, barite concrete samples were been activated with a constant neutron flux at different irradiation times. The samples were then be processed and measured using AMS. The goal was to establish a correlation between the activities of ^{41}Ca and ^{14}C.

4. Experimental Part

4.1 General Procedures and Analytical Methods

4.1.1 Chemicals

Table 3: List of all used chemicals with details of the supply source, their form and purity.

Sum formula	Supply source	Form	Purity
$Ba(NO_3)_2$	Merck „pro analysi"	Powder	$\geq 99\ \%$
$CaCO_3$	Merck „suprapur"	Powder	$\geq 99\ \%$
$NaOH$	VWR „Technical"	Pellets	$\geq 97\ \%$
Na_2CO_3	VWR „ACS reagent grade"	Powder	Not specified
HCl	Fisher Chemical „Laboratory reagent grade"	Aqueous solution (37 %)	Not specified
H_2SO_4	Merck „suprapur"	Aqueous solution (96 %)	Not specified
HF	Merck	Aqueous solution (40 %)	Not specified
HNO_3	VWR „normapur"	Aqueous solution (65 %)	Not specified
$CHBr_3$	Thermo-Scientific	Aqueous solution (96 %)	Not specified

4.1.2 X-ray fluorescence spectroscopy (XRF)

X-ray fluorescence data for the determination of the Ba and Ca concentration in crushed barite concrete were carried out using a mobile X-ray spectrometer from *'XGLab'* and evaluated with the integrated program *'XGLab - X and Gamma Ray Electronics*' from *Bruker Nano Analytics*.

4.1.3 Elemental Analyzer (EA)

The '*vario ISOTOPE select from Elementar Analysensysteme GmbH*' was used for this thesis. This device can characterize samples for their nitrogen, carbon, hydrogen or sulphur content. The concrete samples were measured by Martina Gwozdz from the Institute of Nuclear Physics of the University of Cologne.[10] For the measurements, a total of 12 samples, each containing 60 mg of baryte concrete, were weighed out in small tin boats. The tin boats measured 4x4x11 mm. The barite concrete was previously crushed in a ball mill of the type *"Starbeaker"* from *VWR* for 30 min at 20 Hz with 5 mm balls. 'Dead' graphite was used as blank material.

4.1.4 Accelerator mass spectrometry (AMS)

4.1.4.1 CologneAMS
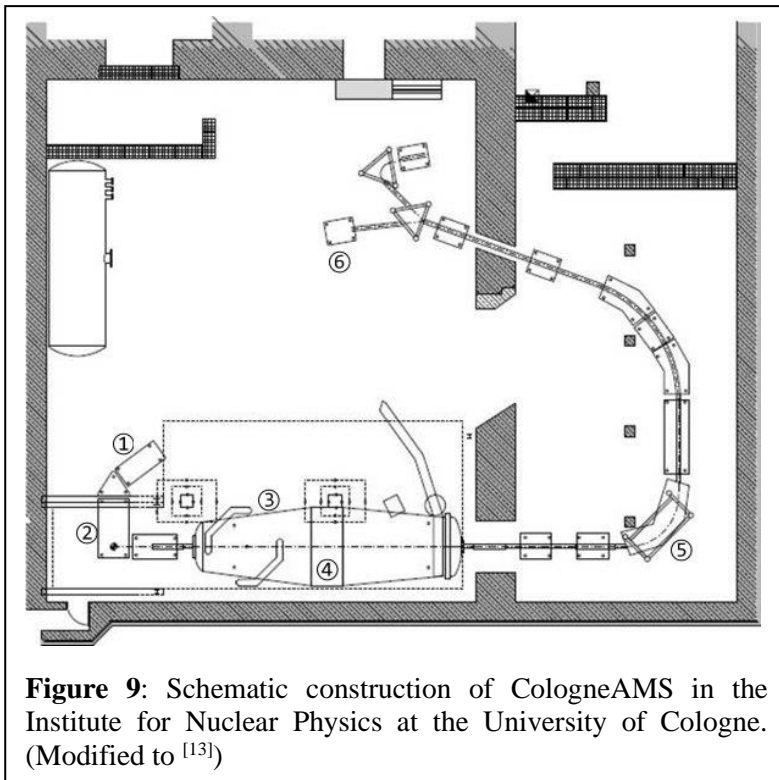
Figure 9: Schematic construction of CologneAMS in the Institute for Nuclear Physics at the University of Cologne. (Modified to [13])

Some of the ^{41}Ca measurements were performed by Stefan Heinze at the 6 MV accelerator of CologneAMS of the Institute of Nuclear Physics of the University of Cologne.[13]

Ag powder was added to the prepared concrete samples beforehand in the ratio 3:1 (powder:sample), pressed into Cu cathodes and placed in a Cs sputter ion source. In the end, the ^{41}Ca/^{40}Ca ratio was determined. A schematic construction of CologneAMS is shown in

Figure 9 with the Cs sputter ion source ①, a 90° magnet for low energy mass separation ②, the 6 MV tandem accelerator ③ with a stripper foil or gas ④, a 90° magnet for high energy mass separation ⑤ and the detector system ⑥.

In addition, other ^{41}Ca measurements were performed at the 3 MV accelerator at VERA at the University of Vienna by Dr. Martin Martschini under the supervision of Dr. Silke Merchel.

In these measurements, chemical treatment of the barite concrete samples was largely dispensed with and the isobaric ^{41}K was neutralized in the ion beam by means of an upstream laser using the so-called Ion Laser InterAction Mass Spectrometry (ILIAMS).[16,17]

4.1.5 Irradiation of the Concrete Samples

The concrete samples were taken from a barite concrete block (heavy concrete), crushed in a ball mill with 5 mm balls to gain a fine powder and irradiated with thermal neutrons at the TRIGA research reactor of the Johannes Gutenberg University in Mainz.[40]

For this purpose, a total of 5 samples, each ~1.7 g (part powder, part solid piece), were prepared in a pneumatic tube and irradiated at different times with a neutron flux of $1.70 \cdot 10^{12}$. The irradiated samples are listed in **Table 4** and a picture of the mortared concrete is shown in **Figure 10**.

Table 4: List of the sample names, irradiation time, weight and the neutron flux.

Sample name	Irradiation time [s]	Weight [g]	Neutron flux [n/cm^2]
BB01	30	1.7	$1.70 \cdot 10^{12}$
BB02	100	1.7	$1.70 \cdot 10^{12}$
BB03	300	1.7	$1.70 \cdot 10^{12}$
BB04	1000	1.7	$1.70 \cdot 10^{12}$
BB05	3000	1.7	$1.70 \cdot 10^{12}$

Figure 10: Heavy concrete samples in their powder form.

4.1.6 Barite concrete

The concrete samples used in this work were taken from a barite concrete block, which has been assembled according to the German standard DIN-25413-2.[41] The admixed proportion of barite (related to 1 m^3) has a volume of 700 l, which makes a weight of 2954 kg at a density of 4.22 kg/l. In the calculations of the Ba concentration, it was assumed that all barite consists of $BaSO_4$.

The heavy concrete used for the irradiation at the TRIGA reactor at the University of Mainz was enriched with barite ($BaSO_4$). This makes barite concrete a special type of concrete that is used in nuclear facilities to better shield against neutrons and γ-rays. This type of concrete is further defined according to DIN 25413-2 [42] and is characterized by a high density of more than 4200 kg/m^3. A barite amount of about 45-54 % must be added to the heavy concrete to be called barite concrete, see DIN 25413-1.[41]

To be able to determine the ^{41}Ca content using AMS, the barite concrete was chemically processed. It is important to mention that the concrete samples were chemically treated differently for the two measurements on the different AMS systems. Chemical treatment of the concrete sample is essential for measurements of ^{41}Ca at the CologneAMS. This is particularly relevant to suppress the isobaric ^{41}K, which is also possible with the 6 MV accelerator during the measurement.

The separation process based on the work of R. Margreiter was used for the chemical treatment; see **Chapter 4.1.7**. The sample preparation for the AMS measurement is described in **Chapter 4.1.4.1**.

4.1.7   Calcium separation procedure

The procedure used in this thesis for the calcium separation from concrete for measurements at CologneAMS is based on the work of Raphael Margreiter in his proposal.[6] He developed the separation of calcium for concrete samples for the measurements by AMS based on the work of Hou.[9] The separation process modified by R. Margreiter was further refined in the process of this work and used in the scheme shown in **Figure 11**, the experimental details are described below.
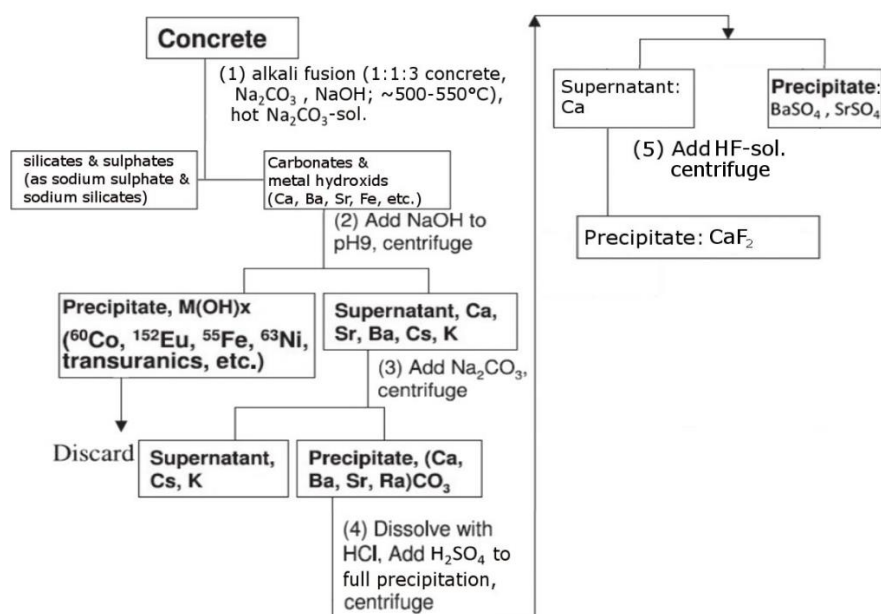
Figure 11: Scheme of the calcium separation procedure of concrete samples used in this work.

In order to make the components in the barite concrete more accessible for chemical processing, a digestion had to be carried out at the beginning. A so-called alkali fusion with NaOH and Na$_2$CO$_3$ and a defined quantity of concrete in a ratio of 3:1:1 (NaOH:Na2CO3:concrete) was used. These components were combined in a defined order in a nickel crucible, see **Figure 12**, and heated in a muffle furnace at 550 °C for 3 hours. After the crucible had cooled to room temperature, forming a green-bluish solid, 10 mL of 0.2 M Na$_2$CO$_3$ was added and the sample was heated on a hot plate to 145 °C with

Figure 12: Order of chemicals in the nickel crucible for the alkali fusion.

occasional stirring. After the sample had dissolved entirely from the crucible, the suspension was transferred to a 15 ml centrifugation tube using a plastic pipette and centrifuged at 3000 rpm for 10 min.

The supernatant was removed and ~3 ml of 4 M HCl was added to the residue. In the process, some components of the concrete residue dissolved. After gas evolution was no longer observed, the suspension was centrifuged at 3000 rpm for 5 min and then the yellow-coloured supernatant was transferred to a new tube by decanting. The supernatant was then adjusted to a pH of 8-9 using 6 M NaOH. The transition group metals were precipitated as hydroxides. It should be noted here that the pH value does not go too high; otherwise the alkaline earth elements will also precipitate.

The supernatant was then separated from the residue by centrifugation (3000 rpm, 5 min) and transferred to a new tube. Depending on the volume, a defined amount of solid Na$_2$CO$_3$ was added to reach a concentration of 0.2 M in the solution. The alkaline earth elements pricipitate out as carbonates, while the alkaline elements, such as potassium, remain in solution as ions. The supernatant was then removed by centrifugation (3000 rpm, 5 min) and the colourless residue was washed with ~2 ml of 0.2 M Na$_2$CO$_3$ solution. The washing process was performed twice in total.

After the supernatant was removed, the residue was dissolved with ~2 ml of 4 M HCl and by adding 4 M H$_2$SO$_4$, the heavy alkaline earth metals, such as barium, were precipitated as sulphates. The suspension was centrifugated at 3000 rpm for 5 min.

The supernatant was transferred to a new tube and the calcium was precipitated as CaF$_2$ by adding 1-2 ml of 40% HF solution. After centrifugation (5000 rpm, 5 min), the supernatant was carefully removed, the residue was washed with 1 ml deionized water and the suspension

was transferred to a 1.5 ml micro reaction vessel. The supernatant was carefully pipetted off after centrifugation (3000 rpm, 5 min) and the residue was dried overnight at 70 °C in a drying oven.

5. Results and Discussion

5.1   Determination of Ca and Ba content in barite concrete

To get information on the concentrations of Ca and Ba in barite concrete, X-ray fluorescence (XRF) measurements were performed on unirradiated concrete in advance. This was also done in order to be able to set expectations of how much Ca can be obtained after the chemical workup and to get a better estimate of the formed ^{41}Ca before the AMS measurements. In addition, the amount of Ba was determined in the heavy concrete for the measurements at the VERA in Vienna. The increased amount of Ba due to the enrichment with baryte could lead to contamination of the ion source and should be separated beforehand. Three reference samples were prepared for the XRF measurements, each with different amounts of $Ba(NO_3)_2$ and $CaCO_3$, which were combined, crushed and homogenized.

The unirradiated barite concrete sample was ground in a VWR *'Star Beaker'* ball mill with five balls (5 mm). The exact weights and composition of the samples are summarized in **Table 13**.

Table 5: Weights and compositions of the samples used for XRF measurements.

Sample	Weight [mg]	Composition $(Ba(NO_3)_2/CaCO_3)$
Reference 1	95.88 $(Ba(NO_3)_2)$ 5.14 $(CaCO_3)$	19:1
Reference 2	90.73 $(Ba(NO_3)_2)$ 10.14 $(CaCO_3)$	9:1
Reference 3	80.52 $(Ba(NO_3)_2)$ 20.15 (CaO_3)	4:1

Barite concrete	100.06

In the XRF analysis, each sample was measured three times. The Kα and Kβ peaks of Ba (32.19 keV and 36.38 keV)[43] and the Kα peak of Ca (3.69 keV)[43] were examined. The respective counts were added for each sample and divided to determine the respective Ca/Ba ratio. The Kβ peak of Ca was not used for the evaluation because its intensity was too low and the peaks of the Ba-Ll energies partially overlapped. An example of the X-ray spectrum of one of the barite concrete measurements is shown in **Figure 13**.
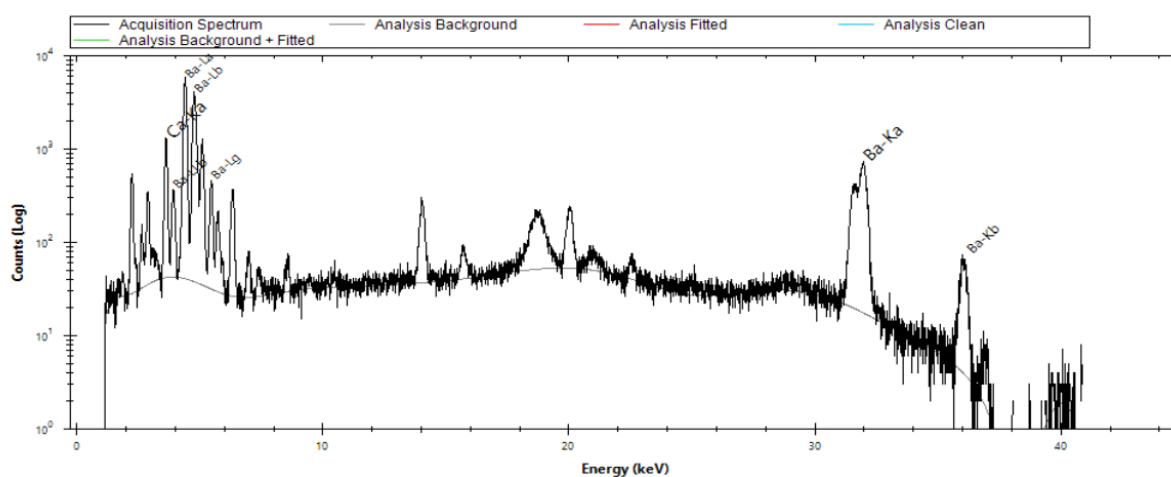
Figure 13: X-ray spectrum of one of the barite concrete measurements. To determine the Ca and Ba concentration, the Ca-Kα peak at 3.69 keV and the Ba-Kα and Ba-Kβ peaks at 32.19 keV and 36.38 keV respectively.

Expected values for the concentrations of Ba and Ca were calculated from the amount of $Ba(NO_3)_2$ and $CaCO_3$ for the reference samples. These values were compared to those from the XRF measurements to provide a reference graph. The Ba/Ca ratio in the barite concrete sample was then determined. The calculated Ca/Ba ratios of the reference samples are shown in **Table 14**, together with the measured values. The plot of the ratios can be seen in **Figure 14**.

Table 6: The calculated and measured Ca/Ba ratio of the three reference samples.

Sample	Calculated Ca/Ba ratio [m/m]	Measured Ca/Ba ratio [Counts]	Error
Reference 1	1:24.48	0.44	± 0.03
Reference 2	1:11.74	0.46	± 0.03
Reference 3	1:5.24	0.71	± 0.03
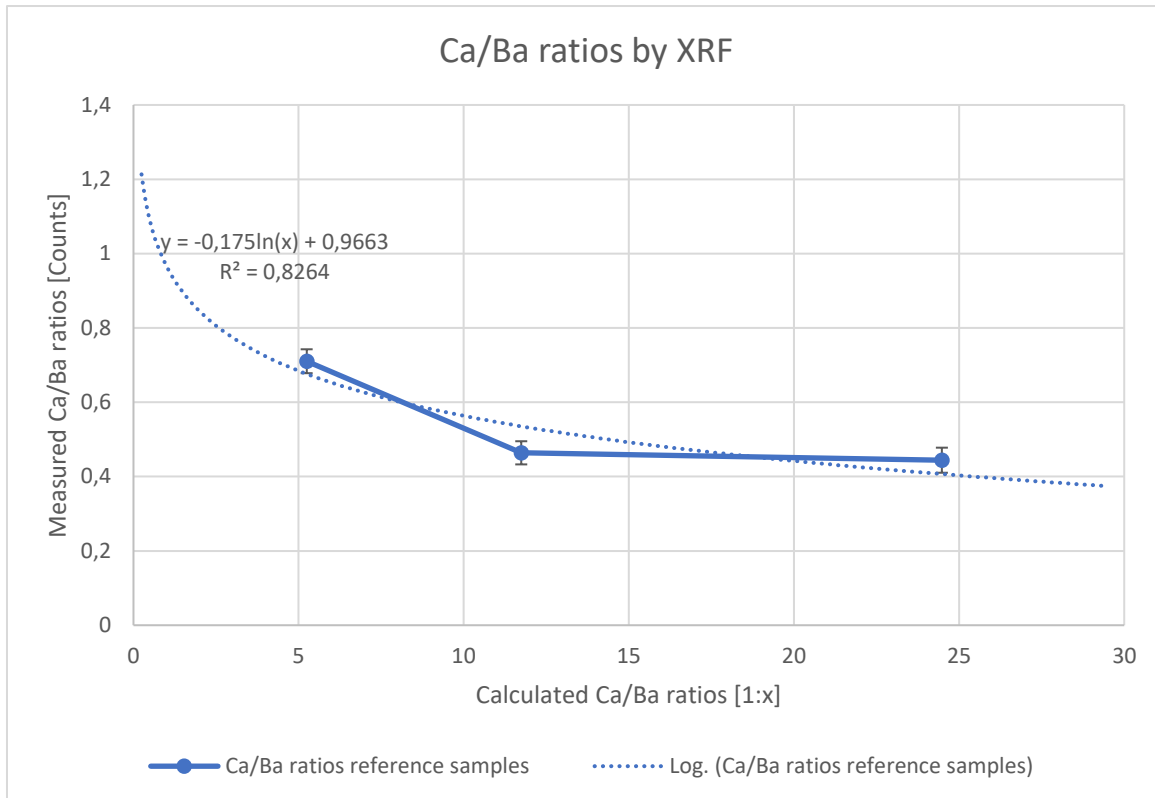
Figure 14: Comparison of the Ca/Ba ratios based on the measured values to the previously calculated Ca/Ba ratios [m/m] of the individual reference samples. Two fits were made, one logarithmic and one using a direct connection of the values. The respective errors are the standard deviations of the values.

The barite concrete sample was also measured three times and the respective counts were added together. The resulting Ca/Ba ratio is 0.47±0.03.

The plot from **Figure 14** shows that the selected fits result in very different relationships. The logarithmic fit gives a Ca/Ba ratio [m/m] of about 1:17, while the direct fit gives a ratio of about 1:8.5. Compared to the ratios from the reference samples in **Table 14**, the concrete sample is closer to *reference 2* than to *reference 1*. For this reason, the value from the direct fit (1:8.5) was used to calculate the Ca concentration.

For the calculation of the Ca concentration, an exact knowledge of the amount of Ba in the barite concrete was required. Since the composition of the heavy concrete was known beforehand and it was mixed according to the German DIN-25413-2 [41], see **Chapter 4.1.6**, the amount of barite and, accordingly, the processed Ba could be determined.

For the calculations, it was assumed that all barite consists of $BaSO_4$. As a result, the amount of Ba was calculated from the amount of barite and scaled down to 100 mg of concrete to better match the sample amount. The calculations made are shown in **equations 4 and 5**.

$$m_{Ba}[kg] = m_{Barite}[kg] * \frac{Amount\ of\ Ba\ in\ BaSO_4\ [\%]}{V_{Barite}\ [l]} \qquad (4)$$

From **equation 4**, the amount of Ba in 1 dm^3 dry heavy concrete is 2.45 kg. This results in 24.83 mg Ba in 1 cm^3 of barite concrete.

In **equation 5**, the amount of Ba per 100 mg (0.422 cm^3) of concrete was calculated.

$$m_{Ba}[mg] = \frac{m_{Ba} \; in \; 1 \; cm^3 \; concrete \; [mg]}{V \; of \; 100 \; mg \; barite \; concrete \; [cm^3]} \tag{5}$$

This calculation yields an amount of 58.84 mg Ba per 100 mg barite concrete. Then the amount of Ba received was offset with the determined Ca/Ba ratio from the XRF measurements to determine the amount of Ca in barite concrete. **Equation 6**, therefore, results in a total amount of 6.93 mg Ca per 100 mg barite concrete.

$$m_{Ca}[mg] = \frac{m_{Ba}\;[mg]}{Ca/_{Ba} ratio \; (direct \; fit)} \tag{6}$$

5.2 Determination of the ^{41}Ca/^{40}Ca ratio by AMS

To determine the ^{41}Ca content, five barite concrete samples were activated for different times with a constant neutron flux. The samples were measured at two AMS systems, at the CologneAMS at the Institute of Nuclear Physics of the University of Cologne and at the VERA in the Faculty of Physics at the University of Vienna.

5.2.1 CologneAMS

5.2.1.1 Irradiated concrete samples

The results of the ^{41}Ca/^{40}Ca measurements are listed in **Table 7** and shown in **Figure 15**.

Table 7: Summary of the ^{41}Ca/^{40}Ca ratios from the AMS measurement (blank corrected) at the CologneAMS of the irradiated barite concrete samples with the irradiation time and the expected ratios. Two of each irradiated sample were prepared for the measurement.

Sample ID	Irradiation time [s]	^{41}Ca/^{40}Ca (calculated)	^{41}Ca/^{40}Ca (measured)	Error [%]
BB01	30	$1.23 \cdot 10^{-11}$	$1.65 \cdot 10^{-11}$	5.1
			$1.63 \cdot 10^{-11}$	5.2
BB02	100	$4.10 \cdot 10^{-11}$	$5.38 \cdot 10^{-11}$	3.8
			$5.31 \cdot 10^{-11}$	3.7
BB03	300	$1.23 \cdot 10^{-10}$	$1.64 \cdot 10^{-10}$	3.3
			$1.65 \cdot 10^{-10}$	3.4
BB04	1000	$4.10 \cdot 10^{-10}$	$5.50 \cdot 10^{-10}$	3.2
			$5.52 \cdot 10^{-10}$	3.2
BB05	3000	$1.23 \cdot 10^{-9}$	$1.61 \cdot 10^{-9}$	3.1
			$1.65 \cdot 10^{-9}$	3.1
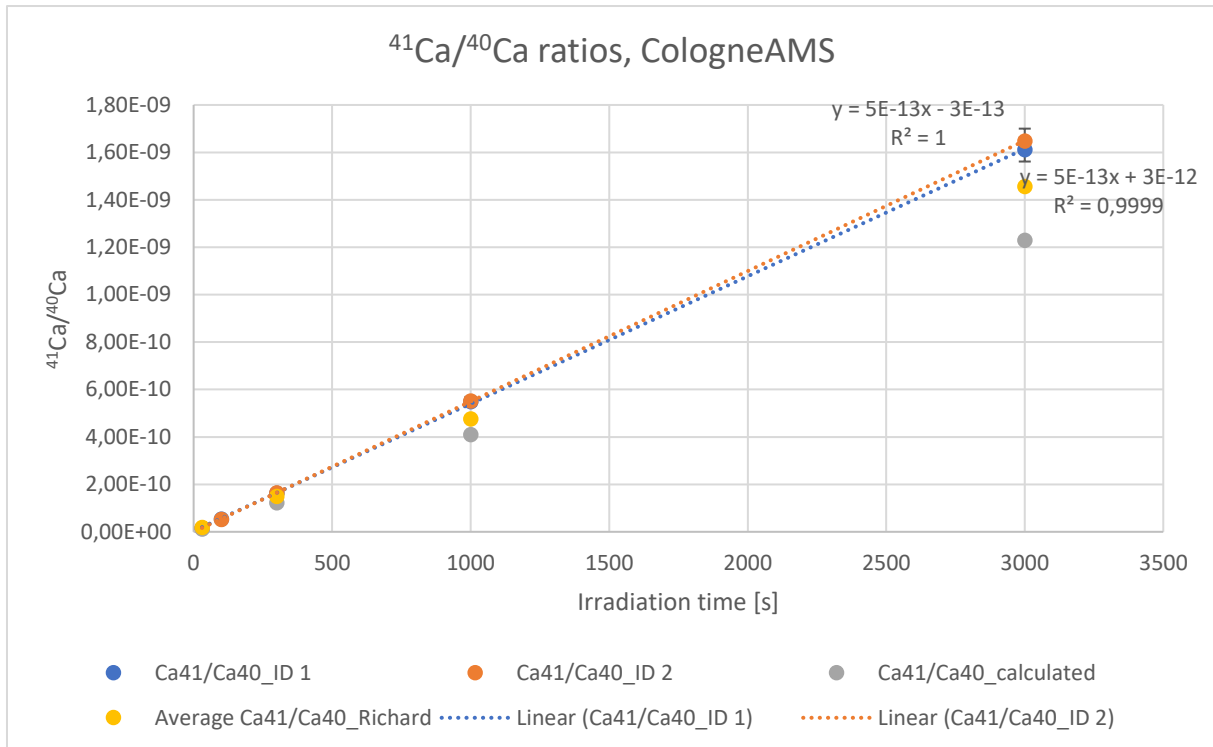
Figure 15: Plot of the measured $^{41}Ca/^{40}Ca$ ratios at the CologneAMS of the baryte concrete samples irradiated at different times with their respective counting rate errors. Both batches were plotted separately and a linear fit was put through the measured values in each case to check the degree of the linear increase and were compared with the results measured by R. Spanier in his dissertation.[5]

In **Figure 15**, it can be seen, that both batches of samples show very well linearity. This is in line with expectations as the amount of ^{41}Ca formed also increases at a constant rate. However, all measured values have a slight deviation from the expected ones. In comparison with the ratios calculated, it is noticeable that the $^{41}Ca/^{40}Ca$ ratio for the baryte sample with an irradiation time of 30 s is slightly lower, while for the longer irradiation times, the values are above the comparative values. However, the deviation is always in the lower percentage range and thus in the tolerant range and in comparison, with the results from R. Spanier, the $^{41}Ca/^{40}Ca$ ratios were reproduced.

In addition to determining the $^{41}Ca/^{40}Ca$ ratio, the activity of ^{41}Ca of the samples irradiated for different times was calculated from these values together with the calculated Ca content in the concrete, see **Chapter 5.1**. For this purpose, the amount of ^{40}Ca [mg/g] in 1 g of barite concrete was first calculated. The proportion of ^{40}Ca in the natural isotope ratio is about 96.4 %.[3] Furthermore, the mass of ^{40}Ca in unirradiated barite concrete was calculated with the Avogadro constant $N_A = 6.022 \cdot 10^{23}$ [44] and the molar mass in order to determine the number of particles $N(^{40}Ca)$, see **equation 7**. By multiplying this by the measured $^{41}Ca/^{40}Ca$ ratios, $N(^{41}Ca)$ can be determined for each sample. Finally, the ^{41}Ca particle number was calculated

with the specific decay constant λ of ^{41}Ca ($2.15 \cdot 10^{-13}$ s^{-1}) and the activity was thus obtained, which is shown in **equation 8**.

The respective activities at the irradiation times are listed in **Table 8** and plotted versus each other in **Figure 16**.

$$N(^{40}Ca) = \frac{m(^{40}Ca) * 0.964}{M(^{40}Ca) * N_A} \tag{7}$$

$$A(^{41}Ca) \left[\frac{Bq}{g}\right] = N(^{40}Ca) * \left.^{41}Ca\right/_{40Ca} * \lambda \ [s^{-1}] \tag{8}$$

Table 8: List of the calculated activities of ^{41}Ca per g of barite concrete from the AMS measurements by CologneAMS of both measurement series for the respective irradiated samples with their respective counting rate errors.

Sample ID	Irradiation time [s]	A(^{41}Ca) [Bq/g] (calculated)	A(^{41}Ca) [Bq/g] (ID 1)	Error [Bq/g] (ID 1)	A(^{41}Ca) [Bq/g] (ID 2)	Error [Bq/g] (ID 2)
BB01	30	$2.68 \cdot 10^{-3}$	$3.67 \cdot 10^{-3}$	$1.87 \cdot 10^{-4}$	$3.63 \cdot 10^{-3}$	$1.88 \cdot 10^{-4}$
BB02	100	$8.93 \cdot 10^{-3}$	$1.18 \cdot 10^{-2}$	$4.46 \cdot 10^{-4}$	$1.16 \cdot 10^{-2}$	$4.34 \cdot 10^{-4}$
BB03	300	$2.68 \cdot 10^{-2}$	$3.57 \cdot 10^{-2}$	$1.19 \cdot 10^{-3}$	$3.60 \cdot 10^{-2}$	$1.21 \cdot 10^{-3}$
BB04	1000	$8.93 \cdot 10^{-2}$	$1.20 \cdot 10^{-1}$	$3.80 \cdot 10^{-3}$	$1.20 \cdot 10^{-1}$	$3.81 \cdot 10^{-3}$
BB05	3000	$2.68 \cdot 10^{-1}$	$3.51 \cdot 10^{-1}$	$1.10 \cdot 10^{-2}$	$3.59 \cdot 10^{-1}$	$1.12 \cdot 10^{-2}$
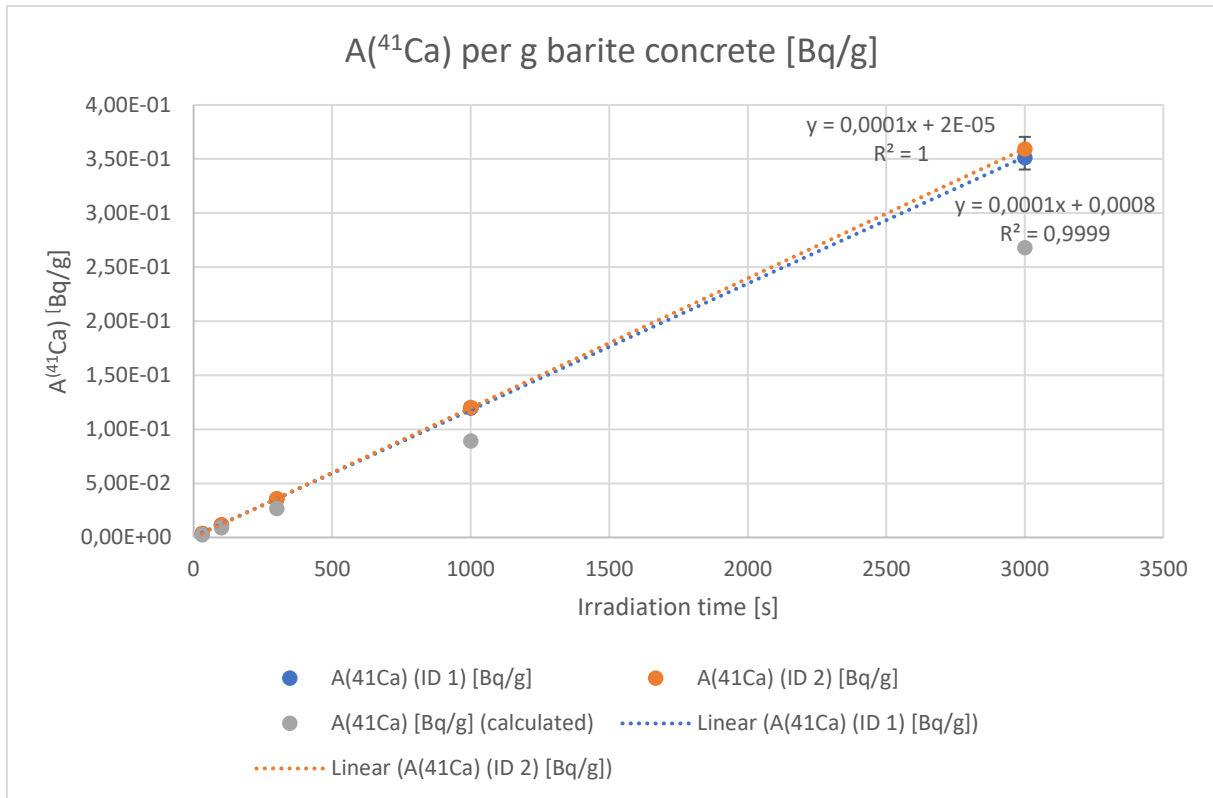
Figure 16: The calculated activities of ^{41}Ca per g baryte concrete with their respective counting rate errors plotted versus the irradiation times [s] from the measurements at CologneAMS. The respective line equations of the series of measurements and the degree of linearity are given.

From the straight lines from the plot in **Figure 16**, a constant increase in activity with longer irradiation times can be seen in both measurements. An activity of about 3.7 mBq/g can be achieved even with a short activation time of 30 s. At 3000 s, this also increases by a factor of about a hundred to about 355 mBq/g.

5.2.1.2 *Dilution series of the irradiated samples*

In addition, a series of dilutions were carried out with the CaF_2 from the separation process using a CaF_2 blank sample. Here it should be investigated whether comparable $^{41}Ca/^{40}Ca$ ratios can be achieved by a targeted dilution of the more highly activated samples to the concentrations of the lower measurement times.

For this purpose, the samples BB02-BB05 were each diluted to the extent that the concentrations of the irradiation times down to BB01. The used CaF_2 "blank" material had a $^{41}Ca/^{40}Ca$ ratio of $5 \cdot 10^{-14}$.

A complete composition of each prepared dilutions is listed in **Table 9**. The diluted samples were measured on the AMS together with the undiluted samples BB01-BB05. The respective $^{41}Ca/^{40}Ca$ ratios are listed in **Table 9** and compared with the mean values of the undiluted

samples. The degree of linearity of the dilution series and the deviation from the undiluted samples is shown in **Figure 17**.

Table 9: Listing of the dilutions with the respective measured $^{41}Ca/^{40}Ca$ ratios, the errors, the undiluted sample assigned to the dilutions and the deviation of the measured values from each other.

Sample ID	$^{41}Ca/^{40}Ca$	Error [%]	Corresponding to undiluted sample…	$^{41}Ca/^{40}Ca$ (Average)	Deviation [%]
BB02_1	$2.82 \cdot 10^{-12}$	6.5	BB01	$1.64 \cdot 10^{-11}$	17
BB03_1	$5.74 \cdot 10^{-11}$	3.5	BB02	$5.35 \cdot 10^{-11}$	107
BB03_2	$1.54 \cdot 10^{-11}$	3.9	BB01	$1.64 \cdot 10^{-11}$	94
BB04_1	$3.79 \cdot 10^{-11}$	4.0	BB03	$1.64 \cdot 10^{-10}$	23
BB04_2	$7.18 \cdot 10^{-12}$	4.9	BB02	$5.35 \cdot 10^{-11}$	13
BB04_3	$2.17 \cdot 10^{-12}$	7.3	BB01	$1.64 \cdot 10^{-11}$	13
BB05_1	$4.64 \cdot 10^{-10}$	3.1	BB04	$5.51 \cdot 10^{-10}$	84
BB05_2	$1.09 \cdot 10^{-10}$	3.3	BB03	$1.64 \cdot 10^{-10}$	67
BB05_3	$3.65 \cdot 10^{-11}$	3.5	BB02	$5.35 \cdot 10^{-11}$	68
BB05_4	$7.29 \cdot 10^{-12}$	4.7	BB01	$1.64 \cdot 10^{-11}$	44
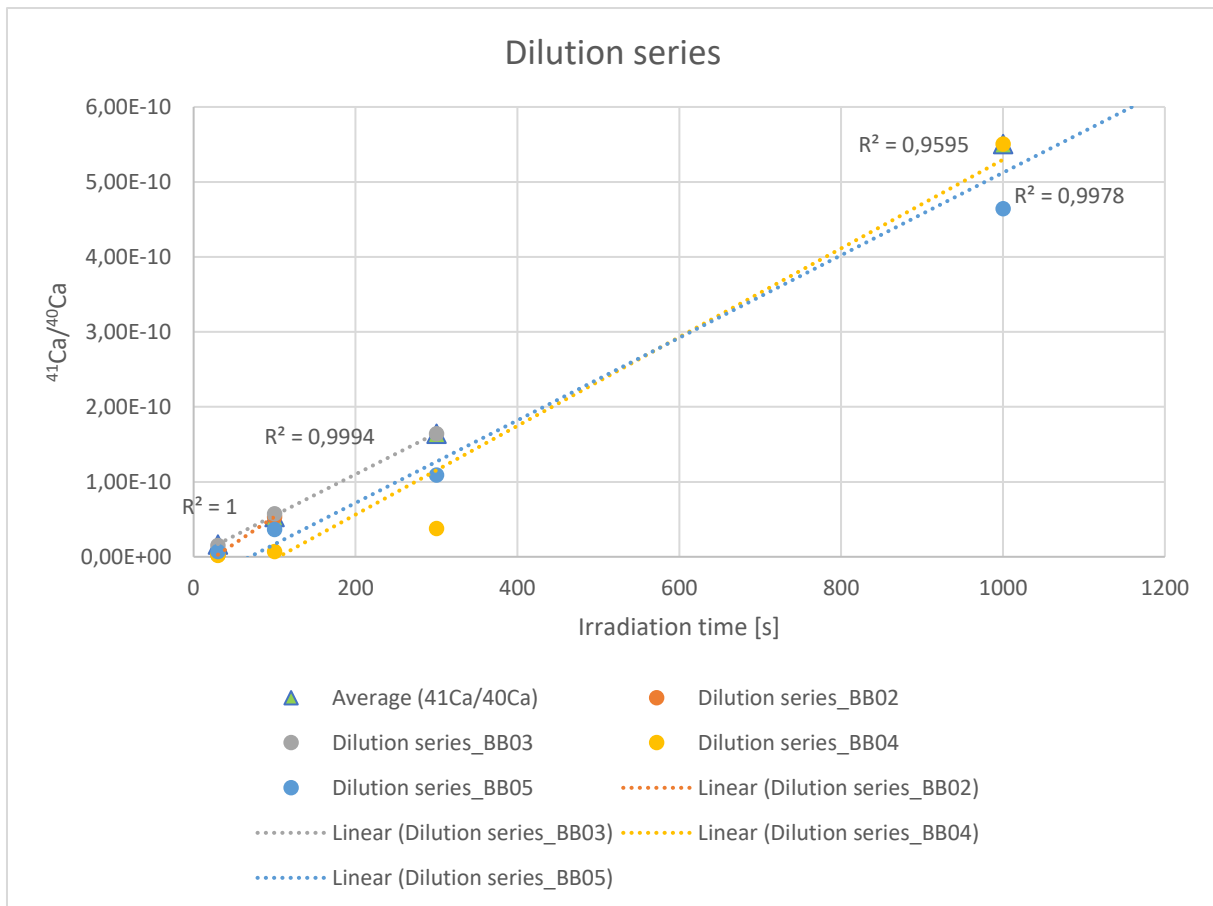
Figure 17: Scheme of the ^{41}Ca/^{40}Ca ratios from the respective dilution series with their respective counting rate errors to the assigned irradiation time [s]. Determination of the linearity of the dilutions and comparison with the values from the original samples.

The measurement results of the ^{41}Ca/^{40}Ca ratios of the dilution series from **Table 9** show a different degree of deviation from the undiluted and expected values. When looking at **Figure 17**, a good linearity can be demonstrated for the respective dilution series, which suggests a constant dilution of the samples. The measurement results can be used to approximate the expected values and thus make a statement about the ^{41}Ca/^{40}Ca concentration. However, due to the relatively high deviation compared to the measured ^{41}Ca/^{40}Ca ratios in **Table 9**, it is not recommended to be used to gain a certain statement. Only a rough estimate of the concentrations to be expected is possible and more worthwhile with longer irradiation times. As a result, lower ^{41}Ca/^{40}Ca ratios can be estimated relatively well with lower irradiation times and possibly also lower neutron fluxes.

5.2.2 VERA

The main feature and an essential difference between the measurements of the ^{41}Ca/^{40}Ca ratio on the CologneAMS and the VERA is the ILIAMS system built into the VERA. As a result, a complex chemical treatment, as required for the CologneAMS, was not necessary. With the ILIAMS system, all isobaric nuclides, primarily ^{41}K for the measurement of ^{41}Ca, could be suppressed from the ion beam through selective laser neutralization of cooled anions. However, a basic chemical treatment was necessary to suppress Ba in the ion source.

Another difference is that the VERA has a 3 MV accelerator installed in the system. Before the actual measurements of the activated heavy concrete, preliminary measurements were performed with unirradiated barite concrete. Therefore, the concrete samples were chemically treated with different solutions, each with different concentrations to dissolve the Ca as much as possible and separate it from the Ba. Also, one untreated concrete sample was measured. The solutions used, their concentrations and the resulting ion currents are shown in **Table 10**.

Table 10: Solvents used for the preliminary measurements of the concrete samples, their concentrations, volumes and the Ca ion current resulting from the measurements at the VERA.

Treatment with…	Concentration [mol/L]	Volume [ml]	Ca ion current
Untreated	-	-	25 nA
HCl	4	5	87 nA
HNO$_3$	4	5	16 nA
Bromoform	96 %	5	10 nA

Based on the results from **Table 10**, it was evident that the best Ca current can be generated when the concrete is leached with HCl and the ion source was not poisoned by Ba. However, this treatment was developed ad hoc and should be studied more systematically in the future.

Therefore, the barite concrete samples were leached with HCl, the supernatant containing the Ca was removed and dried. The resulting $CaCl_2$ was mixed with $PbCl_2$ in a ratio of 1:9 and pressed in Cu cathodes for the measurement.

Two samples were prepared for the measurement from each of the lower irradiated barite concrete (BB01 and BB02). The ^{41}Ca/^{40}Ca ratios measured at VERA, the respective errors and the expected values of the respective irradiated samples are shown in **Table 11**.

A graphical representation of the ratios versus the irradiation time [s] and the comparison with the theoretical values is shown in **Figure 18**.

Table 11: List of the sample IDs with the respective $^{41}Ca/^{40}Ca$ values measured on the VERA and their errors, the irradiation time [s] and the previously expected ratios.

Sample ID	Irradiation time [s]	$^{41}Ca/^{40}Ca$ (calculated)	$^{41}Ca/^{40}Ca$ (measured)	Error [%]
BB01	30	$1.23 \cdot 10^{-11}$	$1.88 \cdot 10^{-11}$	2.8
			$1.74 \cdot 10^{-11}$	5.7
BB02	100	$4.10 \cdot 10^{-11}$	$6.40 \cdot 10^{-11}$	6.8
			$5.45 \cdot 10^{-11}$	3.5
BB03	300	$1.23 \cdot 10^{-10}$	$1.86 \cdot 10^{-10}$	5.4
BB04	1000	$4.10 \cdot 10^{-10}$	$6.03 \cdot 10^{-10}$	5.3
BB05	3000	$1.23 \cdot 10^{-9}$	$1.69 \cdot 10^{-9}$	4.0
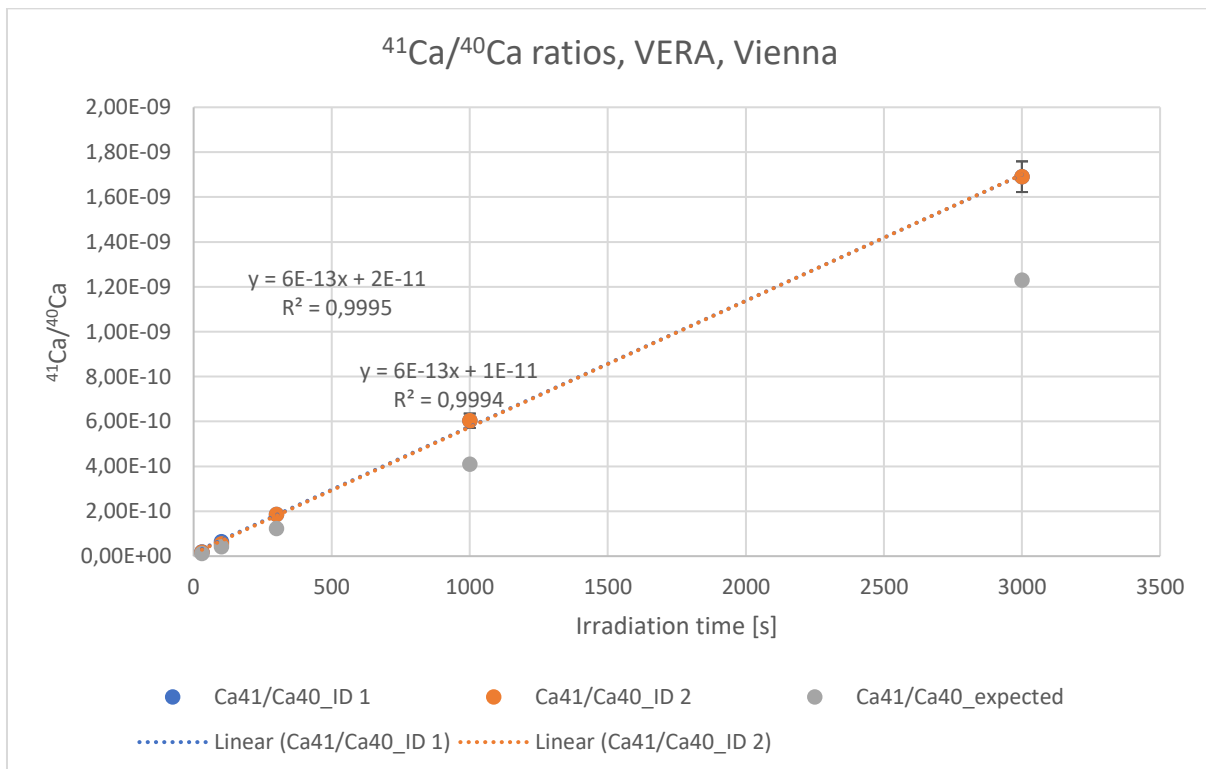
Figure 18: Plot of the measured $^{41}Ca/^{40}Ca$ values with their respective counting rate errors versus the irradiation time [s] of the barite concrete samples. The two series of measurements, ID_1 (*blue*) and ID_2 (*orange*), as well as the previously calculated activities of ^{41}Ca (*grey*), are shown.

The values in **Table 11** and the plot in **Figure 18** show that the ratios of both measurement series are very similar. The errors are also in the lower percentage range. Compared with the expected values, the $^{41}Ca/^{40}Ca$ ratios measured here for the short irradiation time of 30 s are slightly above the values calculated before, but for all other irradiation times above. The

linear increase of the ^{41}Ca concentration can also be observed very constantly for both series of measurements.

Analogous to the ratios from the measurements at CologneAMS, the activity of ^{41}Ca per g of barite concrete was also calculated from the ^{41}Ca/^{40}Ca values measured at VERA. **Formulas 7** and **8** in **Chapter 5.2.1.1** were used for this purpose. The values determined in this way are listed in **Table 12** with the sample ID and the irradiation time and plotted versus each other in **Figure 19**.

Table 12: List of the calculated activities of ^{41}Ca per g of barite concrete from the AMS measurements at VERA of both measurement series for the respective irradiated samples.

Sample ID	Irradiation time [s]	A(^{41}Ca) [Bq/g] (ID 1)	A(^{41}Ca) [Bq/g] (ID 2)	Error [Bq/g] (ID 1)	Error [Bq/g] (ID 2)
BB01	30	$4.10 \cdot 10^{-3}$	$3.80 \cdot 10^{-3}$	$1.13 \cdot 10^{-4}$	$2.15 \cdot 10^{-4}$
BB02	100	$1.39 \cdot 10^{-2}$	$1.19 \cdot 10^{-2}$	$9.49 \cdot 10^{-4}$	$4.10 \cdot 10^{-4}$
BB03	300	$4.06 \cdot 10^{-2}$		$2.18 \cdot 10^{-3}$	$2.18 \cdot 10^{-3}$
BB04	1000	$1.31 \cdot 10^{-1}$		$6.97 \cdot 10^{-3}$	$6.97 \cdot 10^{-3}$
BB05	3000	$3.68 \cdot 10^{-1}$		$1.49 \cdot 10^{-2}$	$1.49 \cdot 10^{-2}$
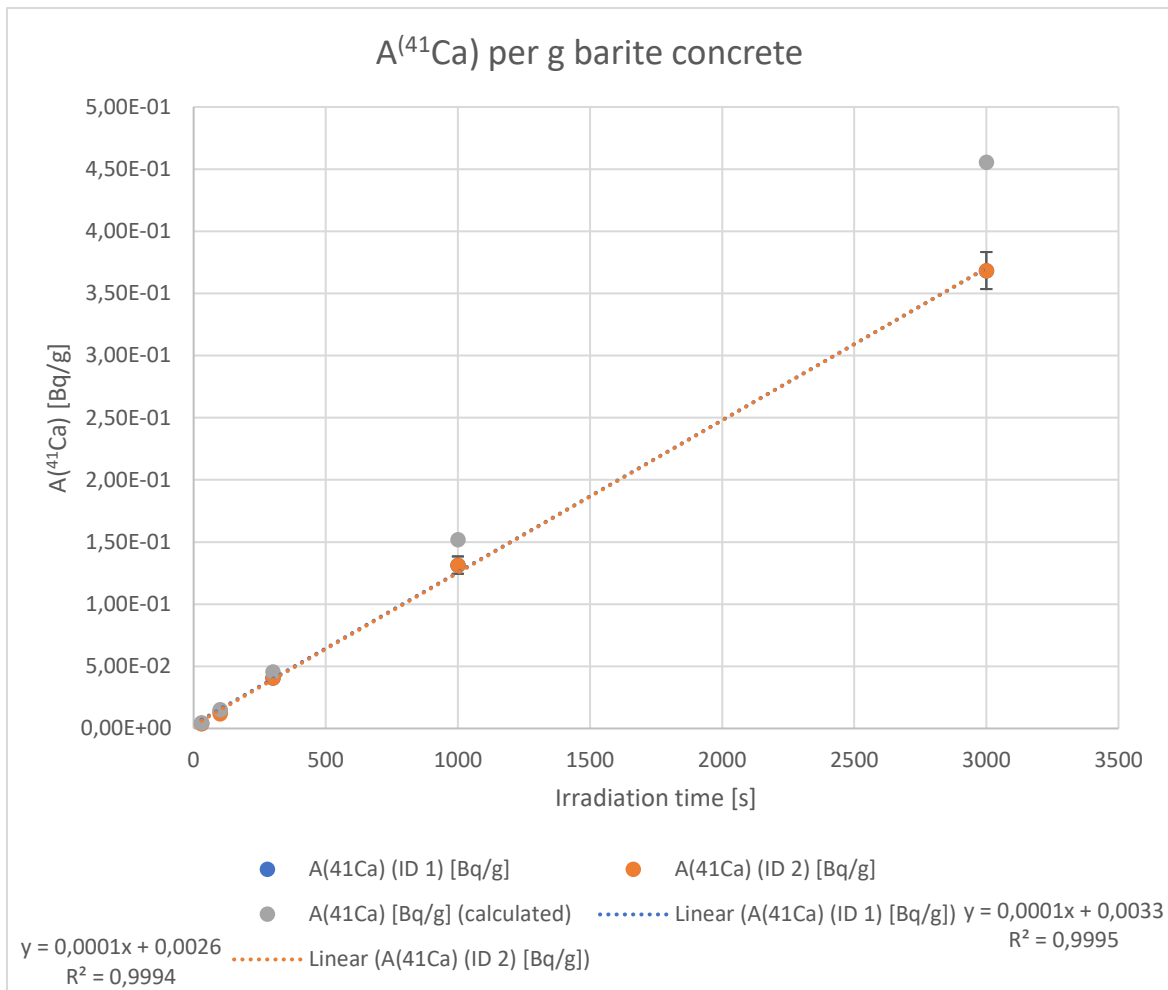
Figure 19: The calculated activities of ^{41}Ca per g baryte concrete with their respective counting rate errors plotted versus the irradiation times [s] from the measurements at VERA. The respective line equations of the series of measurements and the degree of linearity are given.

In **Figure 19**, a constant increase in activity with longer irradiation times can be seen in both measurements. An activity of about 4 mBq/g is achieved at a short activation time of 30 s. Significant differences between the activities of both series of measurements at low irradiation times cannot be observed. At 3000 s, the activity also increases by a factor of about a hundred. The results from **Table 12** and **Figure 19** show that the concentration of ^{41}Ca can be measured very well with the ILIAMS system. This means that the isobar ^{41}K can be suppressed by the laser-assisted system without any complex chemical preparation in advance. However, minimal treatment of the heavy concrete shall be performed to remove the increased amount of Ba caused by the barite due to the risk of contamination of the AMS facility. However, a systematic investigation of possible removal schemes was not performed doing this work.

5.2.3 Comparison of the results from CologneAMS and VERA

Due to the possibility of performing measurements on two different AMS systems, where a different chemical purification was carried out, a comparison of the results is useful. On the one hand, to compare the effect of the different purification methods and, on the other hand, the influence of the different accelerator energies (6 MV and 3 MV) and the ILIAMS system at VERA for the suppression of the isobaric ^{41}K. For this purpose, activities A(^{41}Ca) calculated from the ^{41}Ca/^{40}Ca ratios were averaged and plotted versus the irradiation time, as shown in **Figure 20**. Finally, the deviation from each other was also calculated.
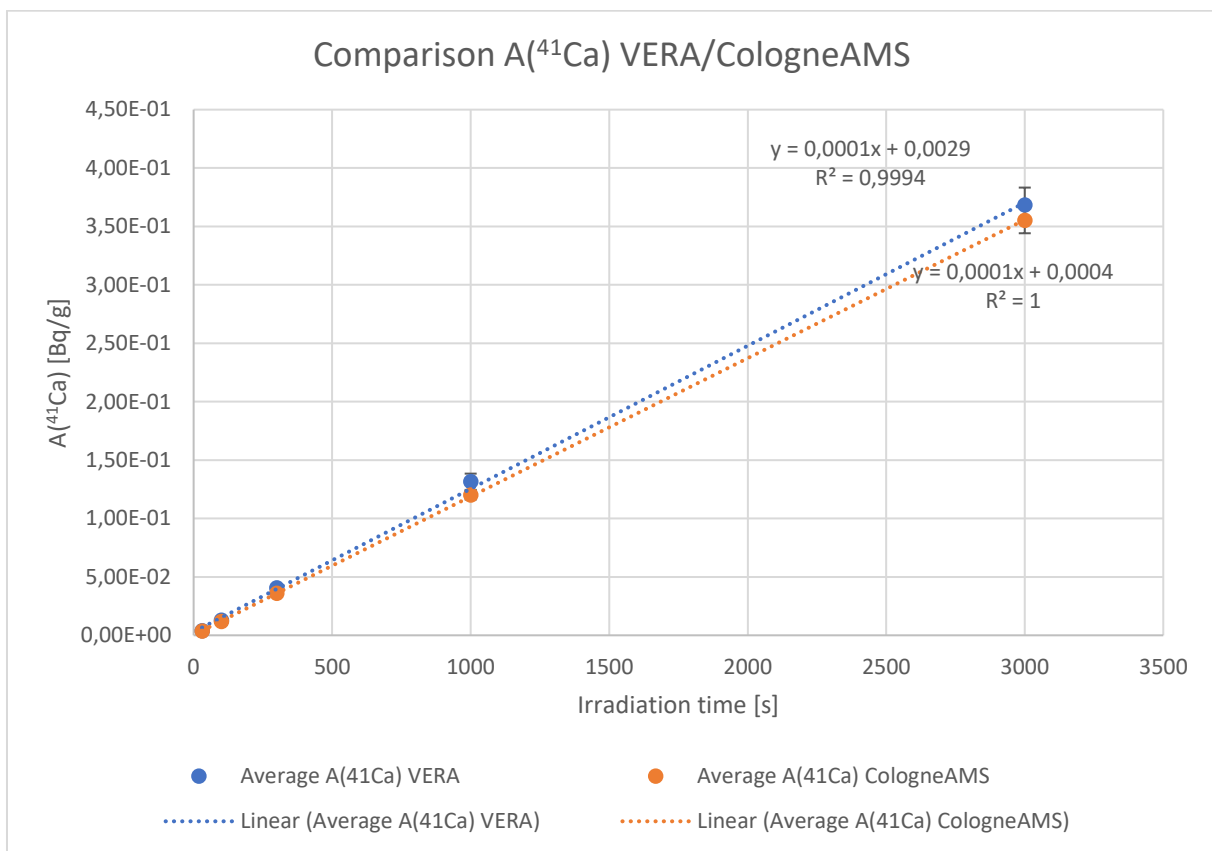
Figure 20: Comparison of the measured activities of ^{41}Ca per g of barite concrete from the AMS measurements at CologneAMS and VERA with their respective average counting rate errors. The activities [Bq/g] are plotted versus the irradiation time [s] and a line was put through the values to show the constant increase.

The comparison in **Figure 20** shows that the activities measured at VERA are slightly higher than at CologneAMS. Nevertheless, the results of both plotted series of measurements are on a similar level and the difference only becomes noticeably larger with longer irradiation times. The mean deviation of the activities between the measurement series is around 8% on average. These results also show that the ^{41}Ca values measured at VERA without complex

chemical treatment are very similar to those at CologneAMS with a complex chemical treatment. Thus, suppression of the isobaric ^{41}K by the ILIAMS system during the measurement is at least as effective as chemically separating the potassium from the concrete beforehand. This shows an effective way to measure ^{41}Ca directly from a heavy concrete sample.

5.3   Determination of the ^{14}C concentration by Elemental Analyser-AMS

In order to investigate a direct connection between the activities of ^{41}Ca and ^{14}C, the irradiated barite concrete samples BB01-BB05, see **Table 4** in **Chapter 4.1.5**, were examined for their carbon content and their ^{14}C concentration. Investigations on the nitrogen content also had to be carried out in advance since most of the ^{14}C formed by neutron capture is produced by the ^{14}N by the nuclear reaction $^{14}N(n,p)^{14}C$.[45] The measurements were performed on an elemental analyser (EA) connected to the CologneAMS in the Institute of Nuclear Physics of the University of Cologne. For this purpose, the concrete, which had previously been crushed in a ball mill (5 mm), was weighed into individual tin boats and folded together without chemical treatment. These tin boats measure 4x4x11 mm. The samples were combusted in the EA and the CO_2 was removed by a helium gas flow. Unfortunately, due to technical difficulties on the EA, the nitrogen concentration of the concrete samples could not be determined in this work specifically, so the work by M. Gwozdz was consulted for comparative values.[10]

To determine the ^{14}C concentration, the $^{14}C/^{12}C$ ratio was determined at the CologneAMS from the irradiated samples and blank material. The values obtained from the measurements are shown in **Table 13**. For each of the irradiated samples, BB01-BB05, two measurements were made. An average N_2 content of ~60 ppm for this type of crushed concrete was used to calculate the expected $^{14}C/^{12}C$ ratios.[10]

From this, the amount of ^{14}N per g of baryte concrete was calculated and further, together with the flux density ($1.7 \cdot 10^{12}$ n/cm^{2}s) and the thermal neutron cross-section of the (n,p) reaction ($1.81 \cdot 10^{-23}$ m^2), the production rate of ^{14}C per second.

Table 13: Sample ID with the associated irradiation times, the calculated expected $^{14}C/^{12}C$ ratios and the values measured at the CologneAMS with their relative counting rate errors. Two series of measurements were prepared and measured from all barite concrete samples BB01-BB05.

Sample ID	Irradiation time [s]	$^{14}C/^{12}C$ (calculated)	$^{14}C/^{12}C$ (measured)	Error [%]
BB01	30	$5.24 \cdot 10^{-12}$	$4.32 \cdot 10^{-12}$	5.5
			$3.90 \cdot 10^{-12}$	4.5
BB02	100	$1.75 \cdot 10^{-11}$	$6.29 \cdot 10^{-12}$	4.5
			$6.08 \cdot 10^{-12}$	4.5
BB03	300	$5.24 \cdot 10^{-11}$	$9.46 \cdot 10^{-12}$	4.5
			$9.41 \cdot 10^{-12}$	4.5
BB04	1000	$1.75 \cdot 10^{-10}$	$4.56 \cdot 10^{-11}$	4.5
			$4.29 \cdot 10^{-11}$	4.5
BB05	3000	$5.24 \cdot 10^{-10}$	$1.73 \cdot 10^{-10}$	4.5
			$2.01 \cdot 10^{-10}$	4.5

Next, the measured values obtained were plotted versus the irradiation time and compared with the previously calculated ratios, see **Figure 21**. For a better comparison, the mean value of each sample was calculated from both measurement series.
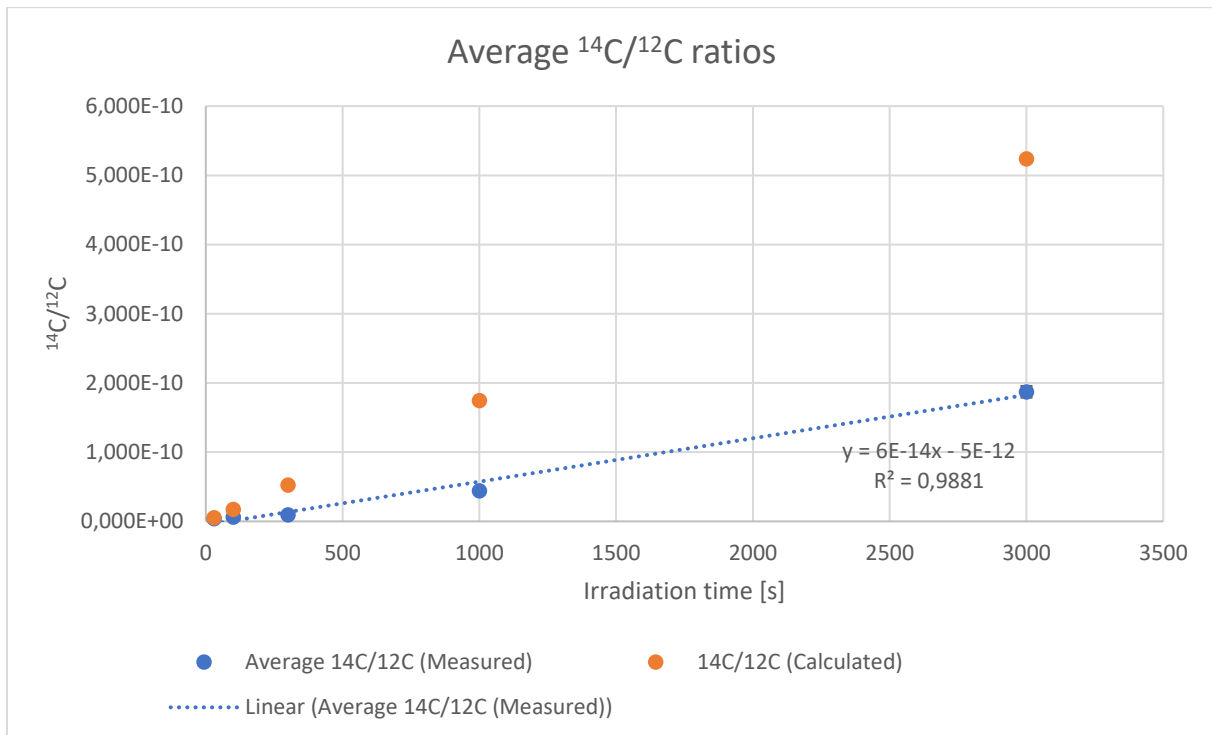
Figure 21: Comparison of the measured $^{14}C/^{12}C$ ratios with their respective counting rate errors with the previously calculated values plotted versus the irradiation time [s]. A linear regression line was put through the values to observe the linearity of the increase and to get a statement about the constancy.

From the values in **Table 13** and more clearly from the plot in **Figure 21,** the measured values deviate significantly from the previously calculated values. This becomes more evident with longer irradiation times. On the one hand, the increase is not as substantial as expected and not that constant in relation to the irradiation time, which can be seen particularly in the lower range of 30 - 300 s. It is also important to observe the comparison of the values at 30 s and 3000 s irradiation time. It was expected that the ratio at 3000 s would be higher by a factor of 100 than at 30 s if the neutron flux remained the same. For 30 s, an average $^{14}C/^{12}C$ ratio of $4.11 \cdot 10^{-12}$ and for 3000 s of $1.87 \cdot 10^{-10}$ was measured. Thus, the activity is only 45 times higher, pointing to a systematised error, due to possible inhomogeneities of the N_2 content.

Table 14: List of the calculated activities of ^{14}C per g of barite concrete from the AMS measurements at CologneAMS of both measurement series for the respective irradiated samples.

| Sample ID	Irradiation time [s]	A(^{14}C) [Bq/g] (ID 1)	Error [Bq/g] (ID 1)	A(^{14}C) [Bq/g] (ID 2)	Error [Bq/g] (ID 2)
BB01	30	$5.65 \cdot 10^{-3}$	$3.13 \cdot 10^{-4}$	$5.08 \cdot 10^{-3}$	$2.29 \cdot 10^{-4}$
BB02	100	$8.38 \cdot 10^{-3}$	$3.78 \cdot 10^{-4}$	$8.09 \cdot 10^{-3}$	$3.64 \cdot 10^{-4}$
BB03	300	$1.28 \cdot 10^{-2}$	$5.75 \cdot 10^{-4}$	$1.27 \cdot 10^{-2}$	$5.71 \cdot 10^{-4}$
BB04	1000	$6.27 \cdot 10^{-2}$	$2.82 \cdot 10^{-3}$	$5.90 \cdot 10^{-2}$	$2.66 \cdot 10^{-3}$
BB05	3000	$2.39 \cdot 10^{-1}$	$1.07 \cdot 10^{-2}$	$2.77 \cdot 10^{-1}$	$1.25 \cdot 10^{-2}$
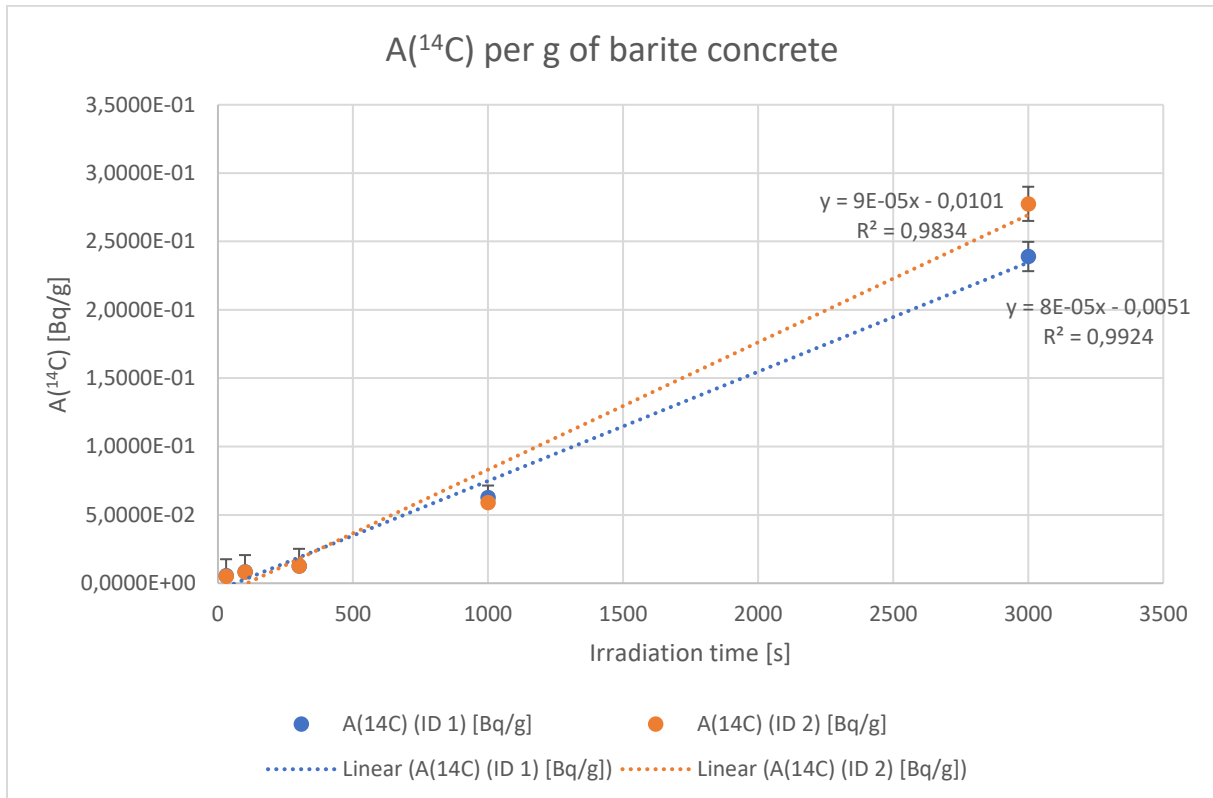
Figure 22: The calculated activities of ^{14}C per g baryte concrete plotted versus the irradiation times [s] from the measurements at CologneAMS with their respective relative counting rate errors. The respective line equations of the series of measurements and the degree of linearity are also given.

The activities determined from the ratios per g of barite concrete of ^{14}C are listed in **Table 14** and plotted versus the irradiation time in **Figure 22**. As with the values of the ratios, no proportionally linear increase in the values can be seen. The results in **Figure 21** also indicate that the linearity of the ^{12}C/^{14}C ratio increases with longer irradiation times. This is also illustrated in the representation of the activity of ^{14}C in **Figure 22**. Based on the results from **Table 14**, the activity increases by a factor of about 10 at the higher irradiation times between BB03 and BB05, depending on the irradiation factor. Thus, short irradiation times seem to be less suitable for an investigation of the formed ^{14}C and only from 300-3000 s of activation a linearity, which can be investigated well, is indicated.

From the work of M. Gwozdz different degrees of crushing with the ball mill or a mortar do not significantly impact the nitrogen concentration, as shown in **Figure 23**. There, the relatively high uncertainty of the N$_2$ concentrations comes into focus. These large uncertainties are also found in the raw data of M. Gwozdz's measurements, errors calculated by standard deviation, which are plotted in **Figure 24**. One assumption as to what might have led to this large area of uncertainty could be an incomplete combustion of the concrete. An

also important significance is the influence of the strength of the helium flow in the EA as a transport gas for nitrogen and carbon. Therefore, a non-uniform mobilization in the gas phase must also be considered.[10]

Another explanation could be found in the system of the EA itself concerning the measurement accuracy. This system is probably not designed for such sensitive analyses in the ppb range, which can lead to a great uncertainty in the measured values, as shown in **Figure 23** and **24**. This has already been described by M. Gwozdz, where the measurements of the blank materials accounted for up to 50% of the values of her samples during her investigations.[10]
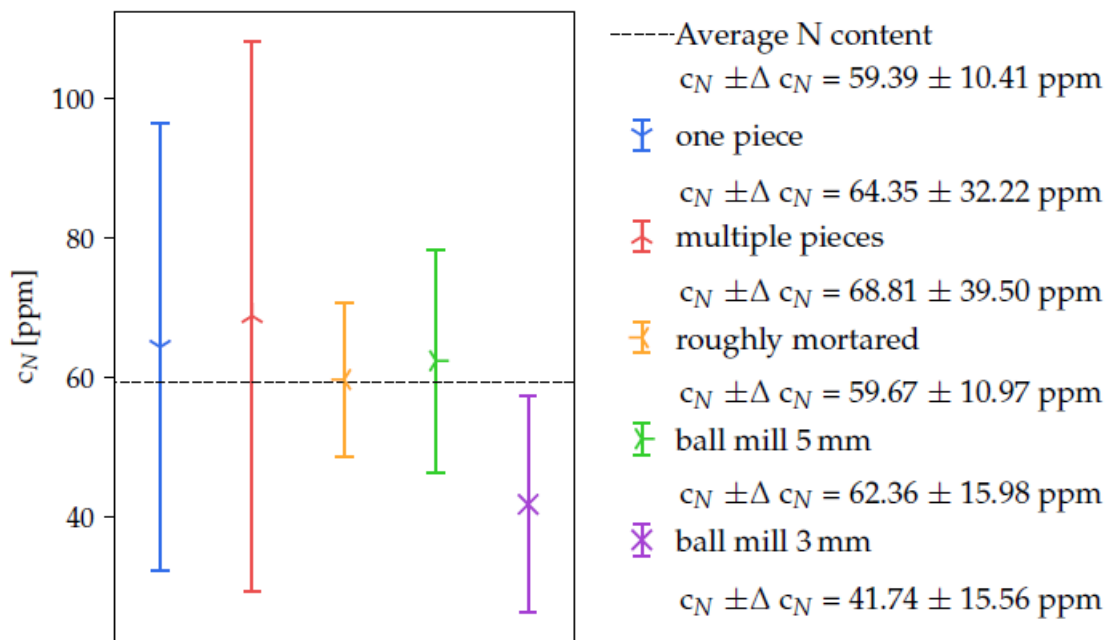
Figure 23: A comparison of differently mortared concrete samples with their average nitrogen contents and their uncertainties from the work of M. Gwozdz.[10]
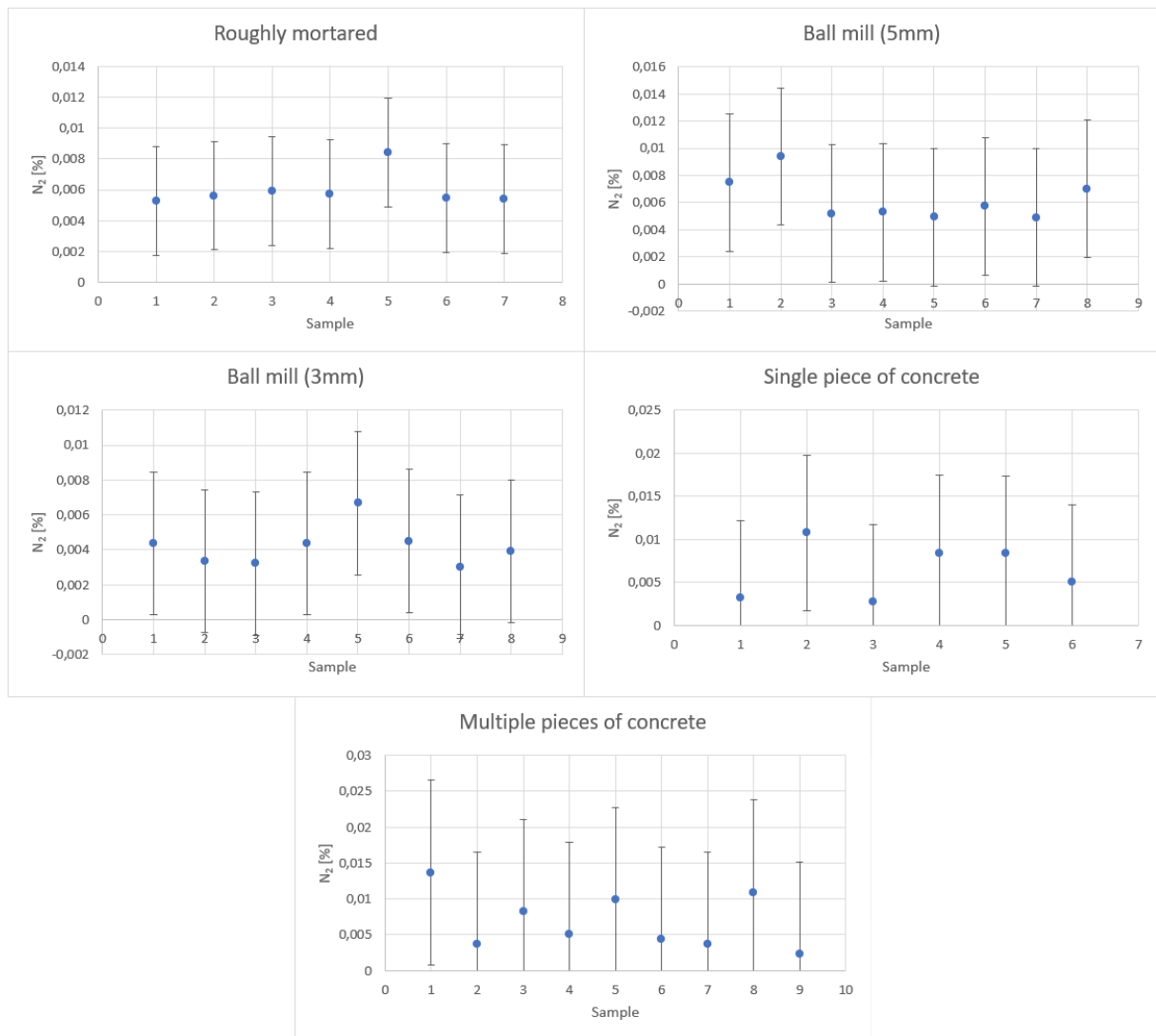
Figure 24: Shown are the measurements at the EA for the differently mortared concrete samples from the work of M. Gwozdz, their respective nitrogen concentrations and their errors calculated by the error propagation of the background counts.[10]

Due to the very large errors in the individual measurements in **Figure 24** of the N_2 concentrations, no concrete prediction of ^{14}C formation and concentration within the concrete is possible. This also makes a reliable correlation with ^{41}Ca very difficult. The uncertainty in the determination of nitrogen could be caused by a systematic error in the measurement (insufficient amount of nitrogen with the same background) or to the inhomogeneous distribution of the pores and ultimately the nitrogen in the concrete.

For measurement accuracy, she specified a quantity of 0.7 µg for carbon and nitrogen, which can be analysed in a comprehensible and reproducible manner with this system.[10]

5.4   Comparison of the activity of ^{14}C and ^{41}Ca

In order to be able to make a statement about a possible correlation between the activity of ^{14}C and ^{41}Ca, these were compared with each other and plotted versus the irradiation time of samples BB01-BB05, in **Figure 25** with the results from the CologneAMS and in **Figure 26** from VERA. It is expected that due to the constant ratio of the effective capture cross-sections of thermal neutrons of ^{14}N(n,p)^{14}C σ = 1.81 barn [38] and ^{40}Ca(n,γ)^{41}Ca σ = 0.41 barn [22], the formation rate will also remain at a constant level at higher irradiation times.
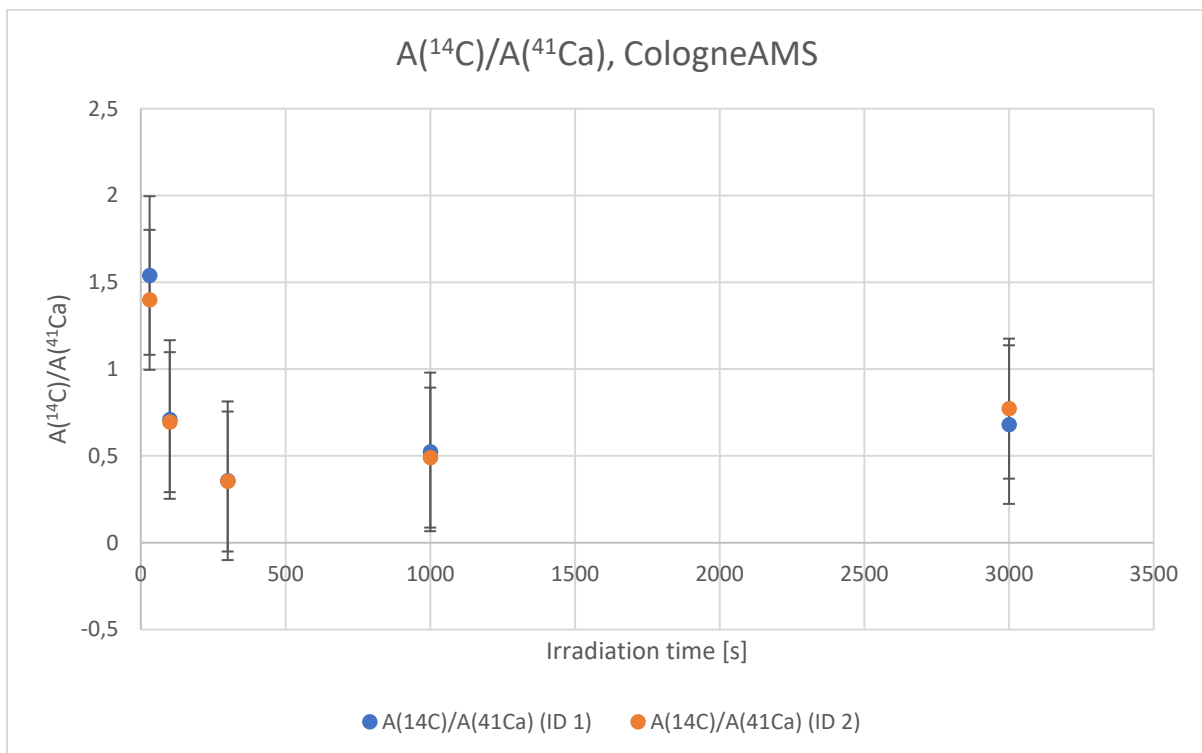
Figure 25: Application of the ratio A(^{14}C)/A(^{41}Ca) from the respective measurement series ID 1 (*blue*) and ID 2 (*orange*) from the CologneAMS measurements to the irradiation times of 30 - 3000 s. The respective errors are the standard deviations of the values.
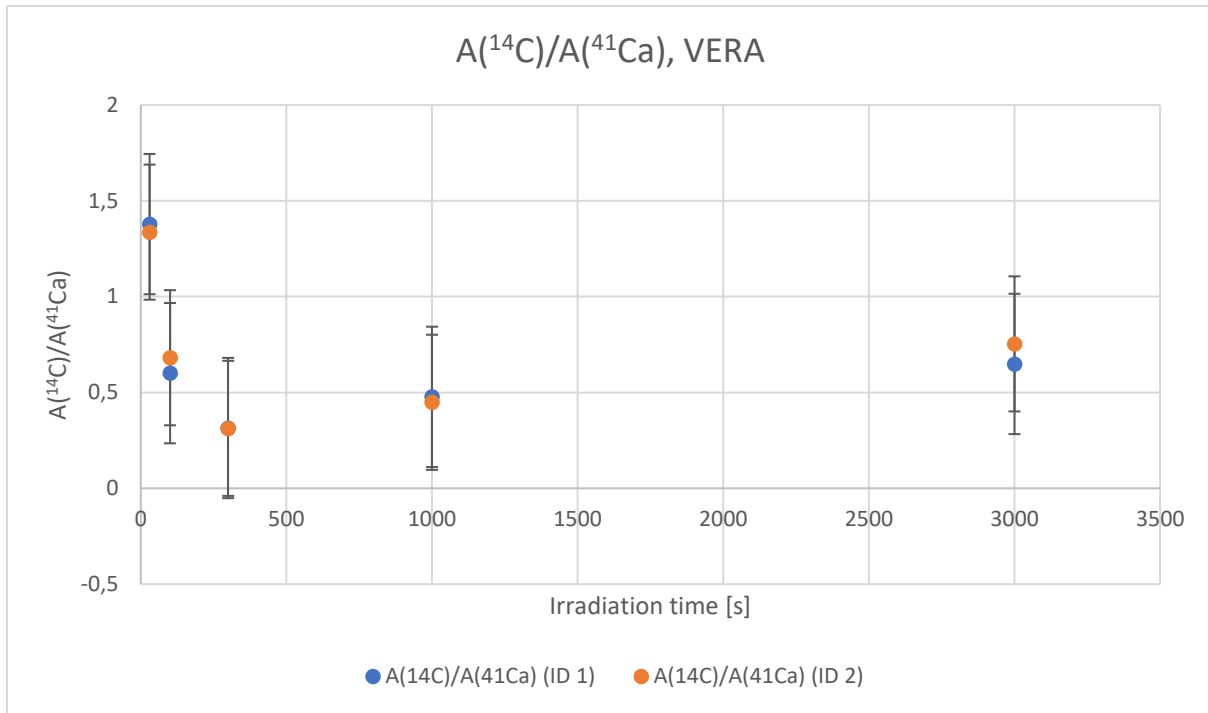
Figure 26: Application of the ratio A(^{14}C)/A(^{41}Ca) from the respective measurement series ID 1 (*blue*) and ID 2 (*orange*) from the VERA measurements to the irradiation times of 30 - 3000 s. The errors are the respective standard deviations of the values.

From the results of the plots in **Figures 25** and **26**, a significant deviation from the expected behaviour is noticeable, with reaching about 50 % deviation of the measured values. In addition, when the focus is put on the measurement points alone, the ratio around one does not show any constancy as expected. This also applies when the uncertainly limits are included. A significant difference between the values of the CologneAMS and the VERA is not noticeable. Both initially show an apparent decrease in the ratio, indicating an increased concentration of ^{41}Ca. The proportion of ^{14}C then increases and the values slowly increase with longer irradiation times.

This comparison of the activities of ^{41}Ca and ^{14}C in **Figures 25** and **26** show that an insufficient correlation between the two radionuclides can be achieved under the conditions examined in this work. The trend shows that a certain dependency can be determined with longer irradiation times. This can already be seen in the results of the individual consideration of the activity of ^{14}C in **Chapter 5.3**. The results of the measurement of ^{41}Ca at VERA with the ILIAMS system from **Chapter 5.2.2** offer the potential of a measurement without chemical treatment of the concrete and without using ^{14}C as a possible vector nuclide for ^{41}Ca. The reason for this deviation is probably that the ^{14}C content could not be measured as reliable as ^{41}Ca as will be discussed in **Chapter 6**.

6. Conclusion and Outlook

6.1 Conclusion

This work focused on three main themes. On the one hand, the establishment of ^{14}C as a proxy for ^{41}Ca. For this purpose, the ^{41}Ca concentration in neutron irradiated concrete was measured at CologneAMS after chemical treatment. A good correlation with the irradiation time could be shown. The measured ^{41}Ca/^{40}Ca ratios agreed well with the calculated values, also reproducing previous results.

The amount of ^{14}C in the irradiated barite concrete was determined using EA-AMS. Based on previous results, some uncertainty in the ^{14}C concentration was expected, but in this work, no unambiguous correlation of activity with the irradiation time could be determined. The possible reason for the large uncertainty of the ^{41}Ca/^{14}C correlation and the ^{14}C measurement itself is the inconsistent mobilization of the nuclide upon combustion in the form of ^{14}CO$_2$, as could be determined by re-evaluating previous measurements of the N$_2$ content in concrete. This hints to systematical uncertainties in the EA measurements of low concentrations, regarding both N$_2$ and ^{14}CO$_2$. However, no final decision can be made from this work as to whether the problems are caused by the inconsistent mobilization from the concrete whether they reflect generally from EA measurements of small concentrations in general.

This picture is further complicated as it can be assumed that ^{14}C is mostly stored in pores as ^{14}CO$_2$ of the barite concrete while the concrete contains about 1 5 of C in solid form incorporated into the structure, so ^{14}C and C might be mobilized differently, agreeing with previous studies of ^{14}C in graphite pores.

Finally, ^{41}Ca was examined in the irradiated concrete at VERA in Vienna using ILIAMS, avoiding complex preparation of the baryte concrete. The results gained at VERA using ILIAMS prove that the isobaric nuclides can be suppressed by this system to such an extent without complex chemical treatment. Only a simplified treatment is necessary to remove a surplus of Ba. Several procedures for this treatment were tested within this work, yet in an exemplary manner. Ehen such a procedure is established systematically, the ^{41}Ca with ILIAMS is straight forward. This would circumvent the additional uncertainty of a ^{14}C proxy arising from the nitrogen determination within the concrete. We conclude that ILIAMS is probably an easier method to investigate the ^{41}Ca concentration than with ^{14}C as proxy.

6.2   Outlook

Considering the results from the comparison of the activities of ^{14}C and ^{41}Ca, future work should focus on the simplified chemical treatment, separating mainly Ba to prevent a malfunction of the ion source.

An further attempt of ^{14}C as a proxy for ^{41}Ca in the measurement of reactor concrete using EA-AMS might be more successful if samples are diluted with additional (inactive) carbon to obtain a reproducible combustion in the EA.

7. Acknowledgement

8. References

[1]   Strahlenschutzverordnung Vom 29. November 2018 (BGBl. I S. 2034, 2036; 2021 I S. 5261), Die Zuletzt Durch Artikel 1 Der Verordnung Vom 8. Oktober 2021 (BGBl. I S. 4645) Geändert Worden Ist, **2018**.

[2]   X. Hou, J Radioanal Nucl Chem **2007**, 273, 43–48.

[3]   J. Magill, R. Dreher, Z. Sóti, Eds. , Karlsruher Nuklidkarte, Nucleonica GmbH, Karlsruhe, **2018**.

[4]   X. Hou, J Radioanal Nucl Chem **2018**, 318, 1597–1628.

[5]   R. Spanier, A 135° Gas-Filled Magnet at the Cologne 10 MV AMS FN-Tandem Accelerator Setup and the Use of 41Ca as a Reference Nuclide for Nuclear Waste Management, Dissertation, University of Cologne, **2019**.

[6]   R. Margreiter, Improving a Separation Procedure for Ca-41 from Heavy Concrete, Research Proposal, University of Cologne, **2018**.

[7]   M. Michel, Verbesserung des Ca-41 Trennungsgangs für AMS-Messungen, Bachelor Thesis, University of Cologne, **2018**.

[8]   J. Lehto, X. Hou, Chemistry and Analysis of Radionuclides: Laboratory Techniques and Methodology, Wiley-VCH-Verl, Weinheim, **2011**.

[9]   X. Hou, Radiochimica Acta **2005**, 93, DOI 10.1524/ract.2005.93.9-10.611.

[10]   M. Gwozdz, Integration of the EA-IRMS System to the Cologne AMS Facility, Master Thesis, University of Cologne, **2021**.

[11]   M. Dewald, B.-A. Dittmann-Schnabel, R. Spanier, Erforschung der Anforderungen an eine radiologische Charakterisierung zur Planung und Durchführung von Stilllegungsmaßnahmen, Gesellschaft Für Anlagen- Und Reaktorsicherheit (GRS) GGmbH, Köln Garching b. München Berlin Braunschweig, **2020**.

[12]   M. Michel, A. Filby, S. Heinze, R. Margreiter, E. Strub, Nuclear Instruments and Methods in Physics Research Section B: Beam Interactions with Materials and Atoms **2022**, 533, 70–75.

[13]   A. Dewald, S. Heinze, J. Jolie, A. Zilges, T. Dunai, J. Rethemeyer, M. Melles, M. Staubwasser, B. Kuczewski, J. Richter, U. Radtke, F. von Blanckenburg, M. Klein, Nuclear Instruments and Methods in Physics Research Section B: Beam Interactions with Materials and Atoms **2013**, 294, 18–23.

[14]   S. Mechernich, T. J. Dunai, S. A. Binnie, T. Goral, S. Heinze, A. Dewald, I. Schimmelpfennig, K. Keddadouche, G. Aumaître, D. Bourlès, S. Marrero, K. Wilcken,

K. Simon, D. Fink, F. M. Phillips, M. W. Caffee, L. C. Gregory, R. Phillips, S. P. H. T. Freeman, R. Shanks, M. Akif Sarıkaya, S. Pavetich, G. Rugel, S. Merchel, N. Akçar, S. Yesilyurt, S. Ivy-Ochs, C. Vockenhuber, Nuclear Instruments and Methods in Physics Research Section B: Beam Interactions with Materials and Atoms **2019**, 455, 250–259.

[15] S. A. Binnie, A. Dewald, S. Heinze, E. Voronina, A. Hein, H. Wittmann, F. Von Blanckenburg, R. Hetzel, M. Christl, M. Schaller, L. Léanni, Aster Team, K. Hippe, C. Vockenhuber, S. Ivy-Ochs, C. Maden, R.-H. Fülöp, D. Fink, K. M. Wilcken, T. Fujioka, D. Fabel, S. P. H. T. Freeman, S. Xu, L. K. Fifield, N. Akçar, C. Spiegel, T. J. Dunai, Nuclear Instruments and Methods in Physics Research Section B: Beam Interactions with Materials and Atoms **2019**, 456, 203–212.

[16] R. Golser, W. Kutschera, Nuclear Physics News **2017**, 27, 29–34.

[17] M. Martschini, D. Hanstorp, J. Lachner, C. Marek, A. Priller, P. Steier, P. Wasserburger, R. Golser, Nuclear Instruments and Methods in Physics Research Section B: Beam Interactions with Materials and Atoms **2019**, 456, 213–217.

[18] M. Schiffer, O. Machhart, A. Priller, S. Herb, G. Hackenberg, S. Heinze, M. Martschini, E. Strub, T. Dunai, R. Golser, A. Dewald, Nuclear Instruments and Methods in Physics Research Section B: Beam Interactions with Materials and Atoms **2022**, 528, 27–33.

[19] J. Lachner, M. Martschini, A. Kalb, M. Kern, O. Marchhart, F. Plasser, A. Priller, P. Steier, A. Wieser, R. Golser, International Journal of Mass Spectrometry **2021**, 465, 116576.

[20] J. Lachner, C. Marek, M. Martschini, A. Priller, P. Steier, R. Golser, Nuclear Instruments and Methods in Physics Research Section B: Beam Interactions with Materials and Atoms **2019**, 456, 163–168.

[21] M. Martschini, J. Lachner, S. Merchel, A. Priller, P. Steier, A. Wallner, A. Wieser, R. Golser, EPJ Web Conf. **2020**, 232, 02003.

[22] F. P. Cranston, D. H. White, Nuclear Physics A **1971**, 169, 95–100.

[23] K. Nishiizumi, M. W. Caffee, D. J. DePaolo, Nuclear Instruments and Methods in Physics Research Section B: Beam Interactions with Materials and Atoms **2000**, 172, 399–403.

[24] J. A. Suárez, M. Rodríguez, A. G. Espartero, G. Piña, Applied Radiation and Isotopes **2000**, 52, 407–413.

[25] K. C. Welten, D. J. Hillegonds, J. Masarik, K. Nishiizumi, Nuclear Instruments and Methods in Physics Research Section B: Beam Interactions with Materials and Atoms **2007**, 259, 653–662.

[26] S. P. H. T. Freeman, B. Beck, J. M. Bierman, M. W. Caffee, R. P. Heaney, L. Holloway, R. Marcus, J. R. Southon, J. S. Vogel, Nuclear Instruments and Methods in Physics Research Section B: Beam Interactions with Materials and Atoms **2000**, 172, 930–933.

[27] H. Shen, F. Pang, S. Jiang, M. He, K. Dong, L. Dou, Y. Pang, X. Yang, X. Ruan, M. Liu, C. Xia, Nuclear Instruments and Methods in Physics Research Section B: Beam Interactions with Materials and Atoms **2015**, 361, 643–648.

[28] Internationale Atomenergie-Organisation, Ed. , Radiological Characterization of Shut down Nuclear Reactors for Decommissioning Purposes, International Atomic Energy Agency, Vienna, **1998**.

[29] S. Hosoya, K. Sasa, T. Matsunaka, T. Takahashi, M. Matsumura, H. Matsumura, M. Sundquist, M. Stodola, K. Sueki, Nuclear Instruments and Methods in Physics Research Section B: Beam Interactions with Materials and Atoms **2017**, 406, 268–271.

[30] T. Schulze-König, C. Maden, E. Denk, S. P. H. T. Freeman, M. Stocker, M. Suter, H.-A. Synal, T. Walczyk, Nuclear Instruments and Methods in Physics Research Section B: Beam Interactions with Materials and Atoms **2010**, 268, 752–755.

[31] D. Hampe, B. Gleisberg, S. Akhmadaliev, G. Rugel, S. Merchel, J Radioanal Nucl Chem **2013**, 296, 617–624.

[32] P. Scholz, Working Title "Determination and Modification of the Quantitative Yield of Ca from Heavy Concrete," University of Cologne, **2023**.

[33] G. Jörg, Y. Amelin, K. Kossert, C. Lierse v. Gostomski, Geochimica et Cosmochimica Acta **2012**, 88, 51–65.

[34] G. A. Kovaltsov, A. Mishev, I. G. Usoskin, Earth and Planetary Science Letters **2012**, 337–338, 114–120.

[35] H. Godwin, Nature **1962**, 195, 984–984.

[36] J. R. Arnold, W. F. Libby, Science **1949**, 110, 678–680.

[37] V. F. Sears, Neutron News **1992**, 3, 26–37.

[38] G. C. Hanna, D. B. Primeau, P. R. Tunnicliffe, Can. J. Phys. **1961**, 39, 1784–1806.

[39] W. von Lensa, D. Vulpius, H.-J. Steinmetz, N. Girke, D. Bosbach, B. Thoauske, A. W. Banford, D. Bradbury, B. Grambow, M. J. Grave, A. N. Jones, L. Petit, G. Pina, Kernkraftwerke in Deutschland: Betriebsergebnisse **2011**, 56, 263–269.

[40] K. Eberhardt, C. Geppert, Radiochimica Acta **2019**, 107, 535–546.

[41] DIN 25413-1:2013-04, Klassifikation von Abschirmbetonen Nach Elementanteilen_-Teil_1: Abschirmung von Neutronenstrahlung, Beuth Verlag GmbH, **2013**.

[42] DIN 25413-2:2013-04, Klassifikation von Abschirmbetonen Nach Elementanteilen_-Teil_2: Abschirmung von Gammastrahlung, Beuth Verlag GmbH, **n.d.**

[43] W. T. Elam, B. D. Ravel, J. R. Sieber, Radiation Physics and Chemistry **2002**, 63, 121–128.

[44] P. Becker, Rep. Prog. Phys. **2001**, 64, 1945–2008.

[45] M.-S. Yim, F. Caron, Progress in Nuclear Energy **2006**, 48, 2–36.
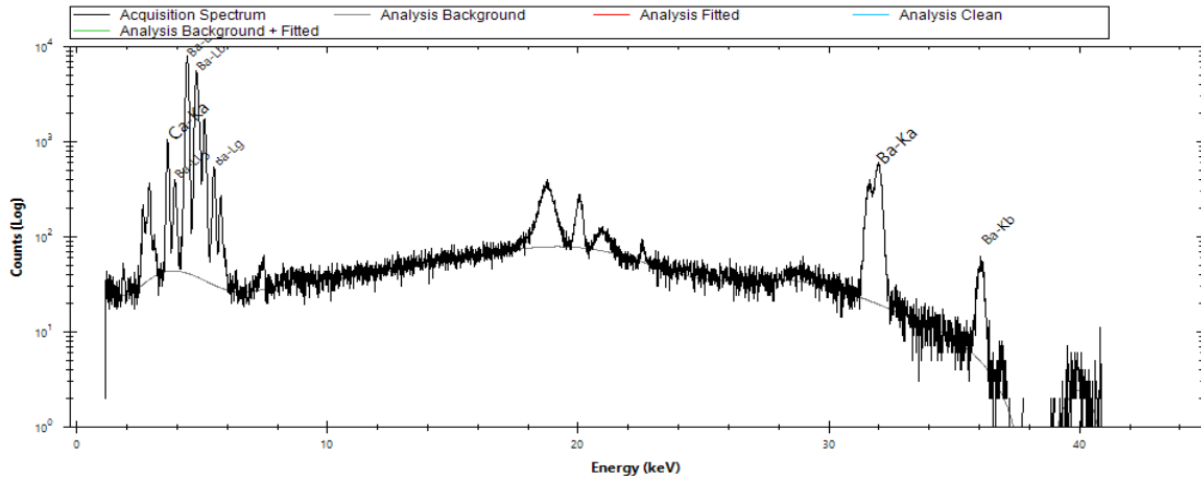
9. Appendix

9.1   XRF spectra

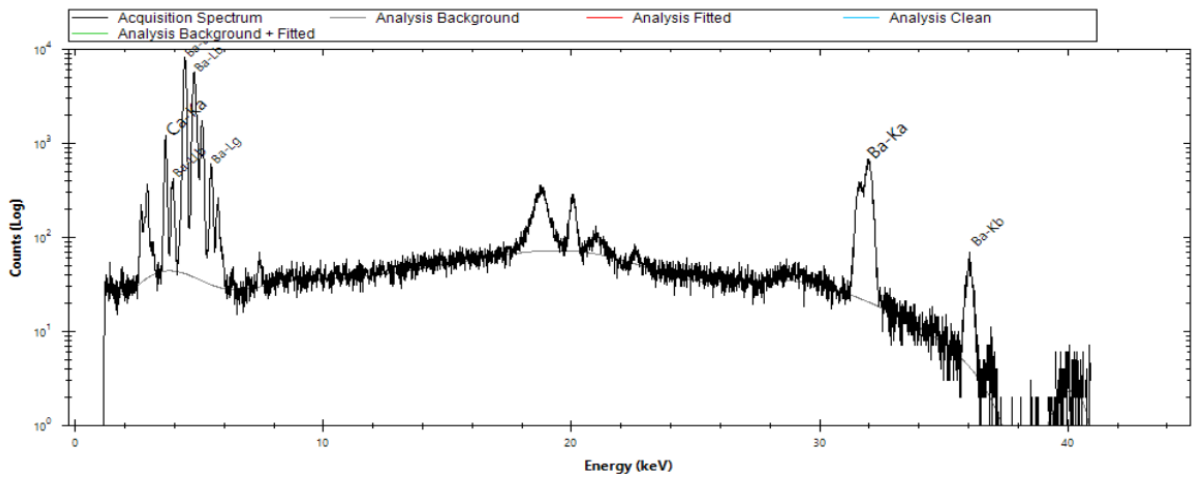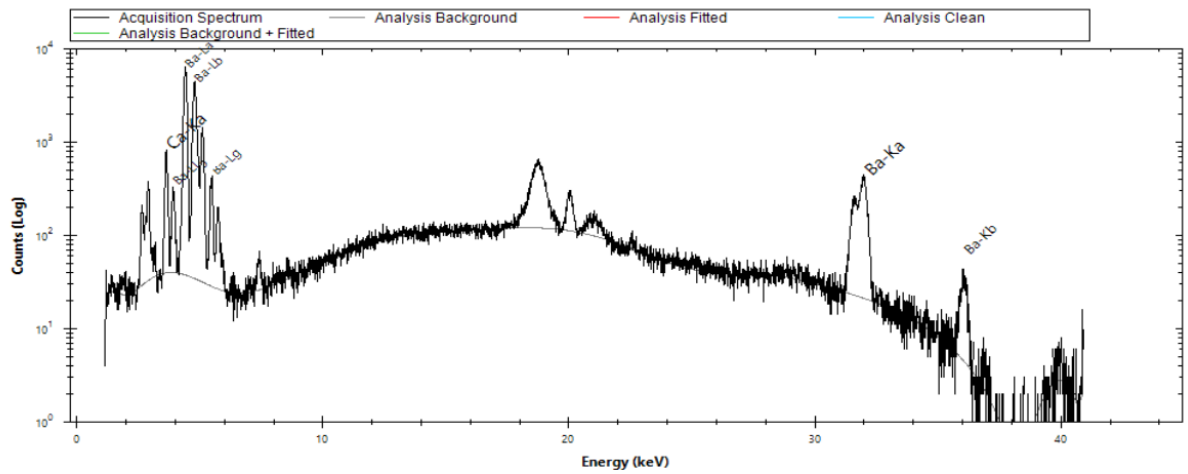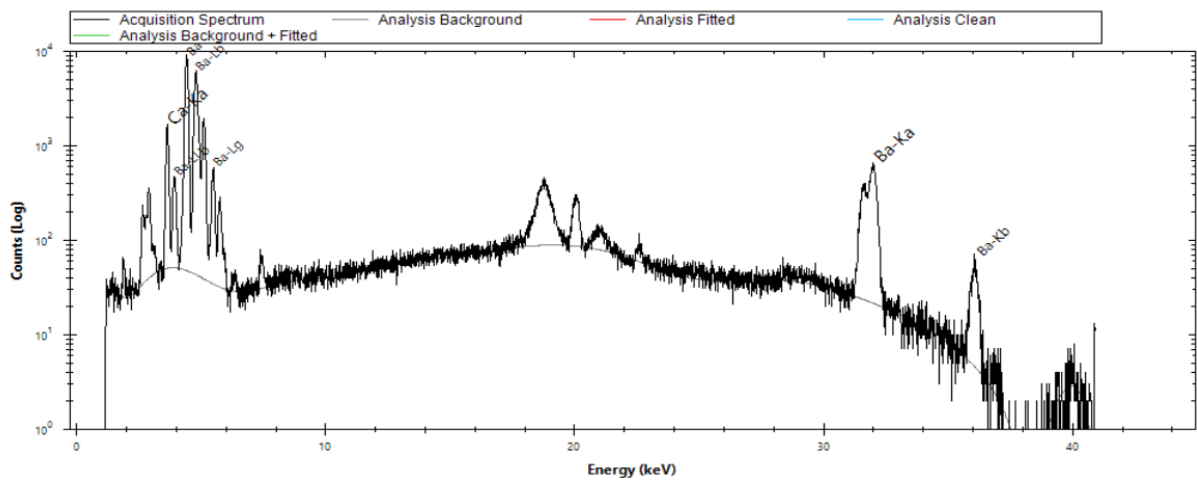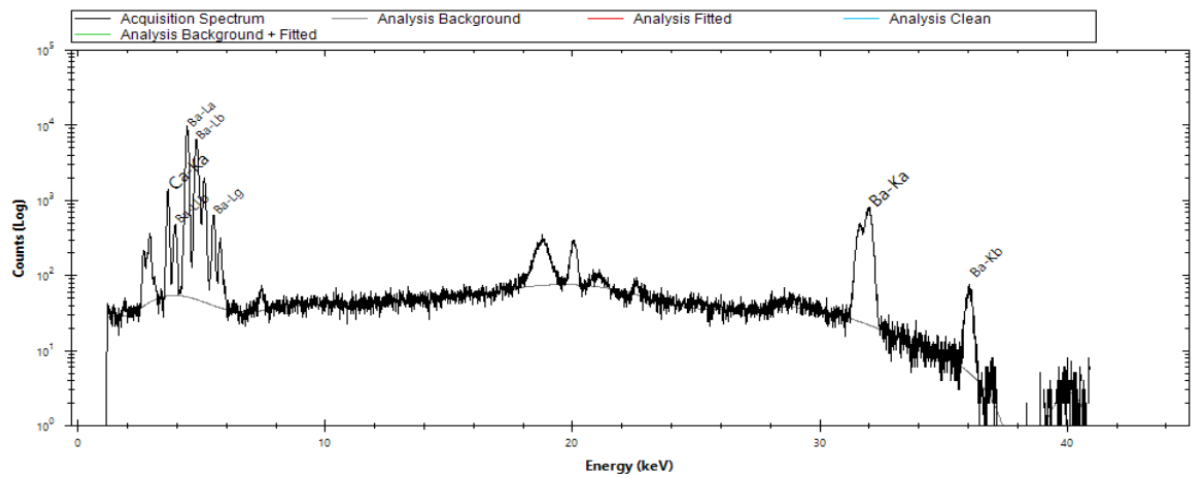**Figure 27**: XRF spectrum of the first measurement of reference sample 1.

Figure 28: XRF spectrum of the second measurement of reference sample 1.

Figure 29: XRF spectrum of the third measurement of reference sample 1.

Figure 30: XRF spectrum of the fourth measurement of reference sample 1.

Figure 31: XRF spectrum of the first measurement of reference sample 2.
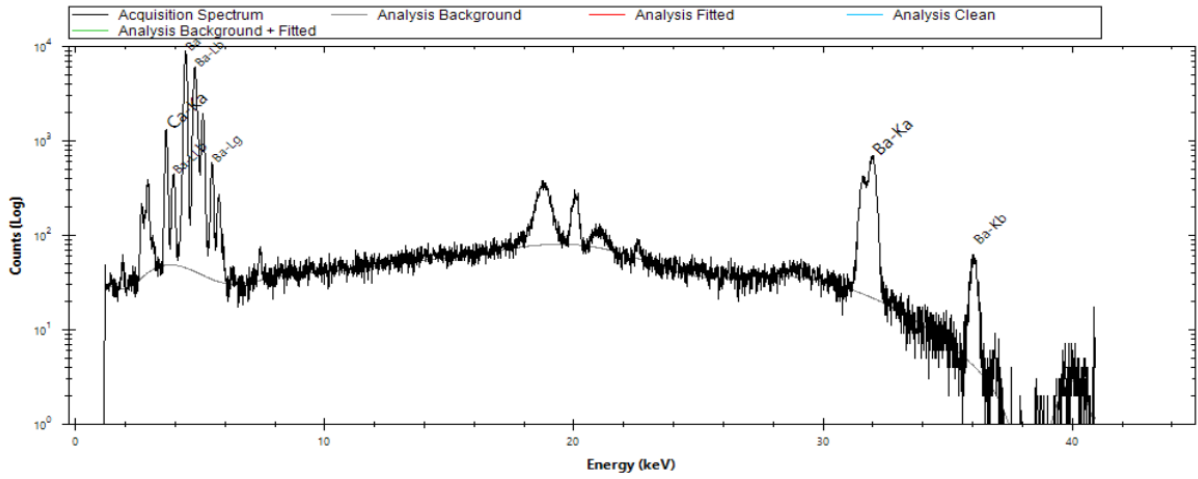
Figure 32: XRF spectrum of the second measurement of reference sample 2.
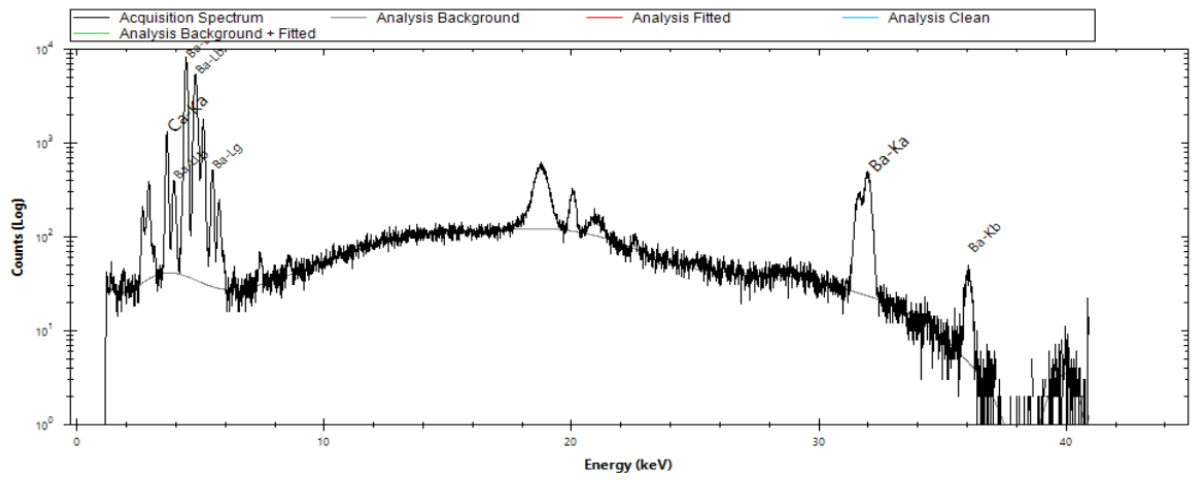

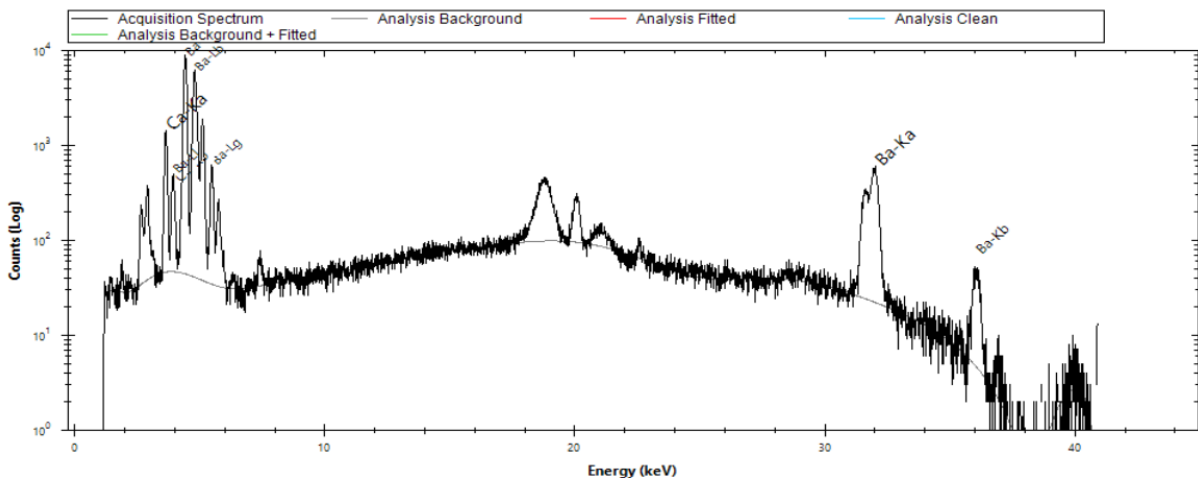**Figure 33**: XRF spectrum of the third measurement of reference sample 2.

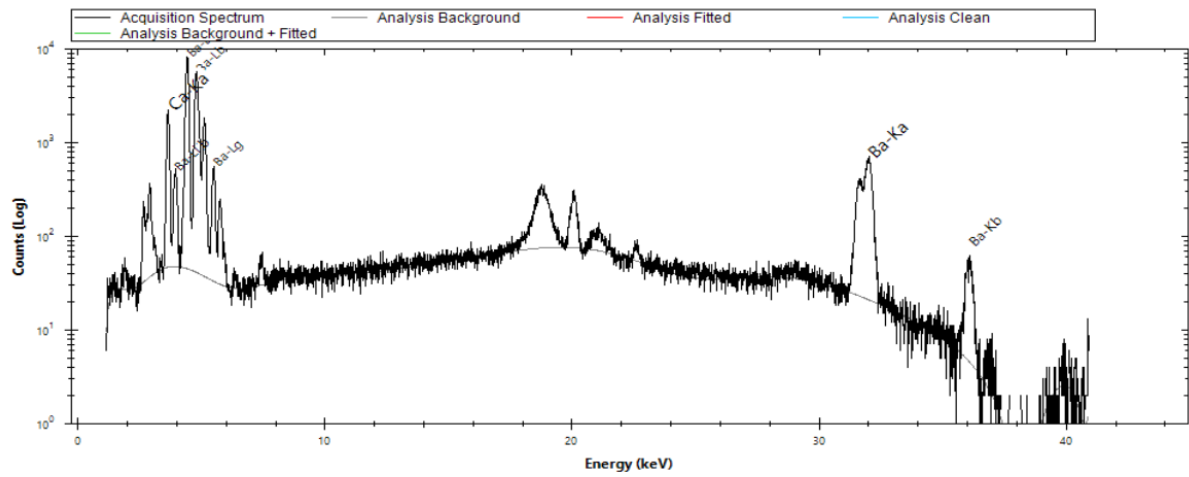**Figure 34**: XRF spectrum of the fourth measurement of reference sample 2.

Figure 35: XRF spectrum of the first measurement of reference sample 3.
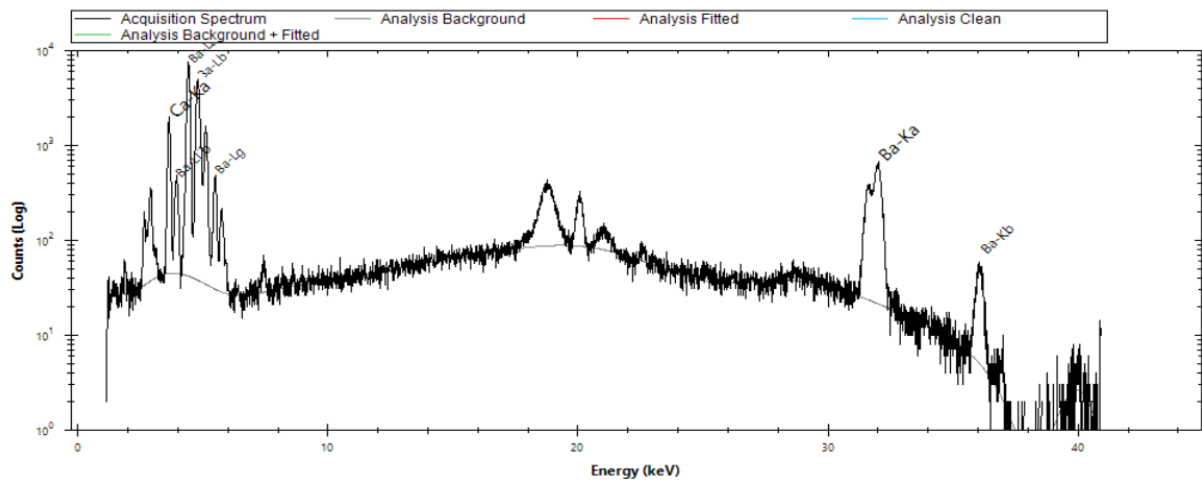

Figure 36: XRF spectrum of the second measurement of reference sample 3.
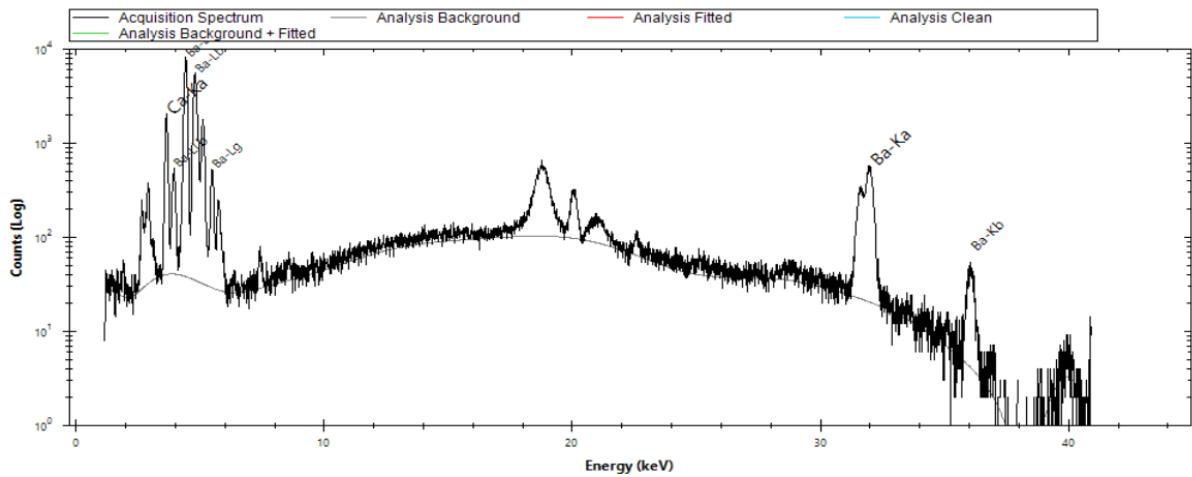
Figure 37: XRF spectrum of the third measurement of reference sample 3.

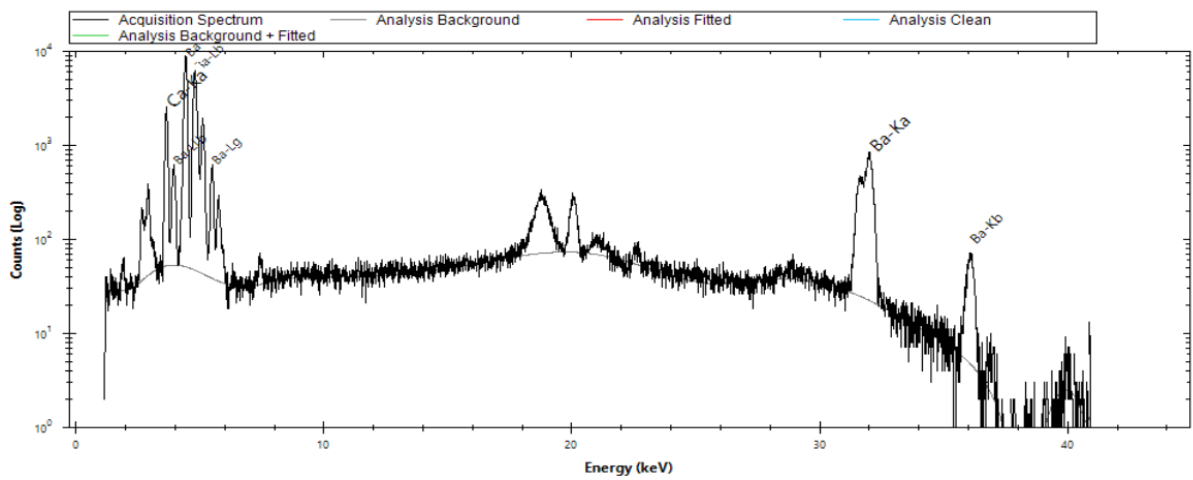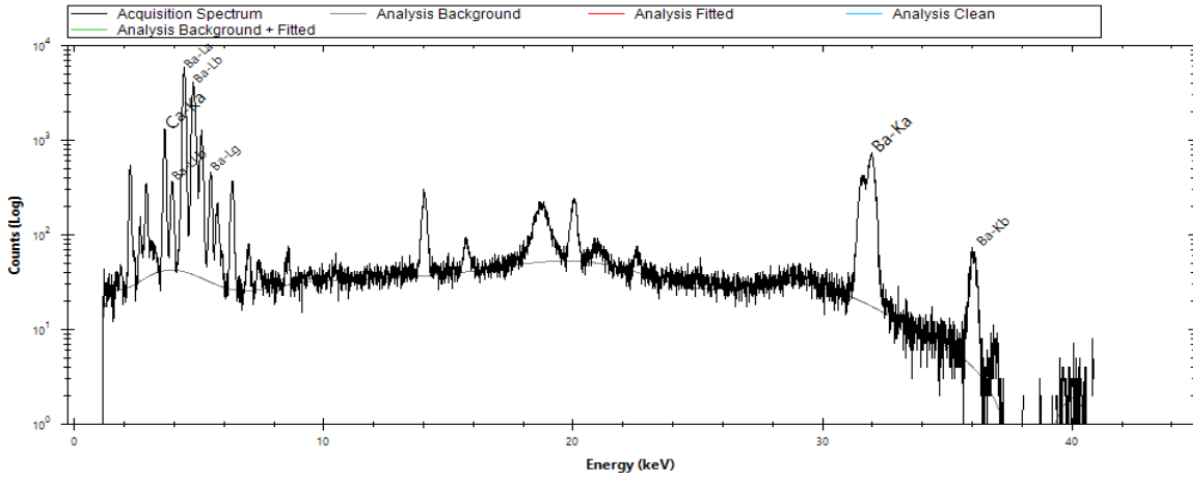**Figure 38**: XRF spectrum of the fourth measurement of reference sample 3.

Figure 39: XRF spectrum of the first measurement of the barite concrete.
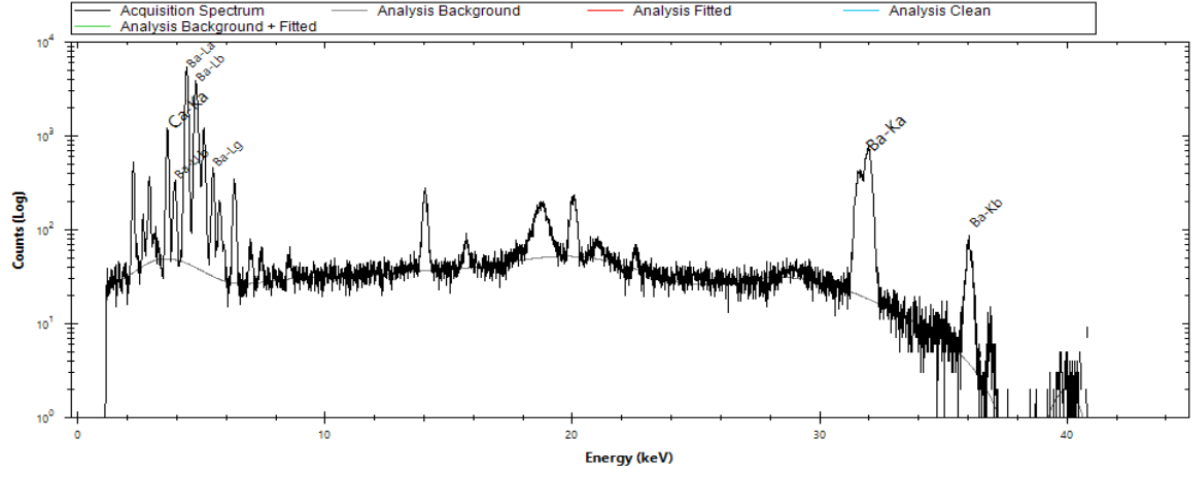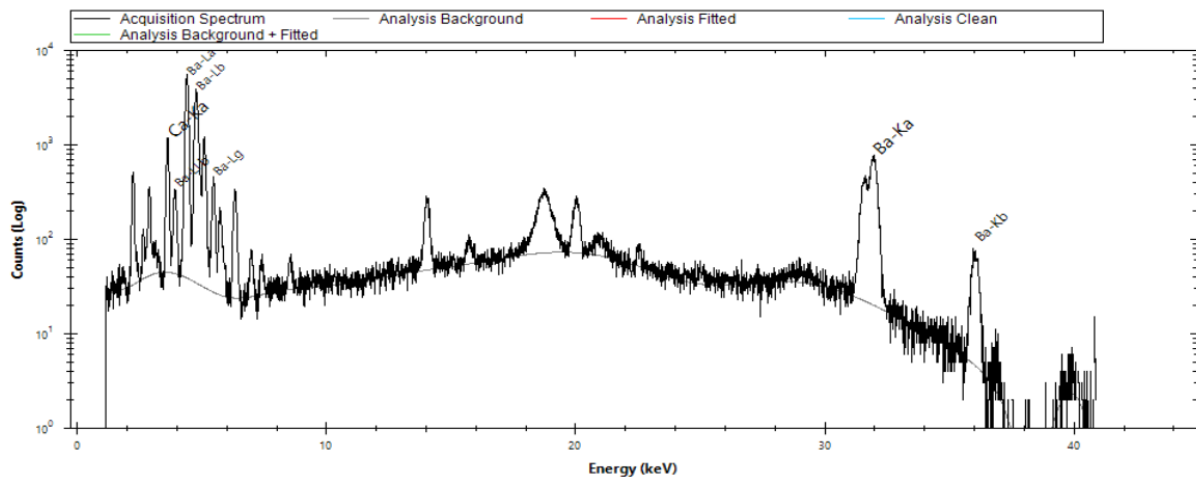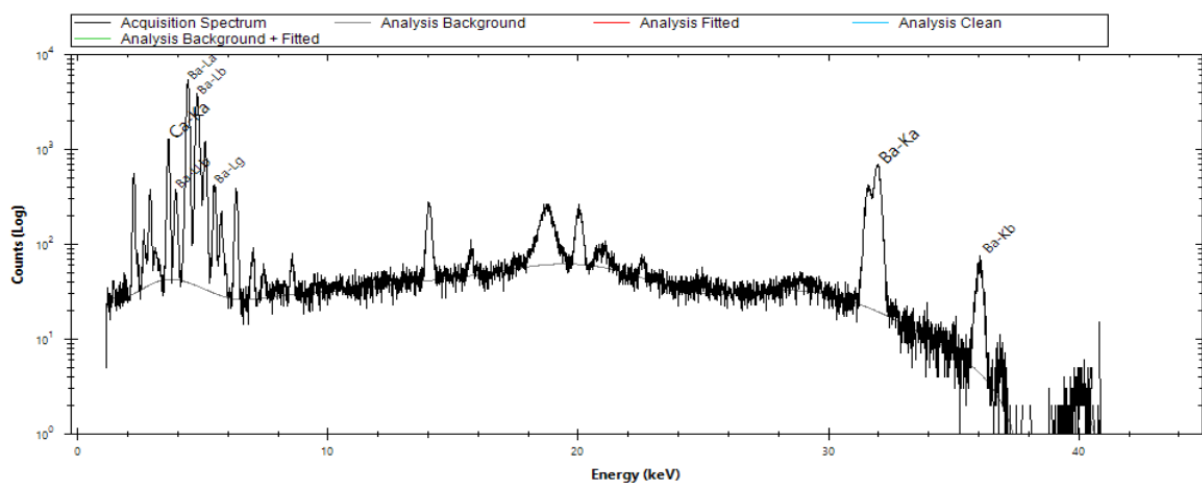

Figure 40: XRF spectrum of the second measurement of the barite concrete.

Figure 41: XRF spectrum of the third measurement of the barite concrete.

Figure 42: XRF spectrum of the fourth measurement of the barite concrete.

9.2 Measured ^{41}Ca/^{40}Ca ratios

Table 15: Measured ^{41}Ca values from the irradiated barite concrete samples at VERA.

Sample-ID	^{41}Ca/^{40}Ca (measured)	uncert.	Rel. uncert. [%]	average ^{40}Ca^{3+} current [nA]
Blank1_1	9.04E-13	1.11E-13	12.28	25.5
Blank1_2	4.59E-13	9.22E-14	20.11	19.3
Blank2_1	2.30E-12	1.74E-13	7.57	37.6
Blank2_2	1.72E-12	2.00E-13	11.67	36.6
Blank3_1	--	--	--	--
Blank3_2	1.37E-12	3.99E-13	29.05	11.0
BB01_1	1.88E-11	5.20E-13	2.76	21.8
BB01_2	1.74E-11	9.85E-13	5.65	21.2
BB02_1	6.40E-11	4.36E-12	6.80	11.5
BB02_2	5.45E-11	1.88E-12	3.46	36.4
BB03	1.86E-10	9.98E-12	5.36	7.6
BB04	6.03E-10	3.20E-11	5.31	9.3
BB05	1.69E-09	6.83E-11	4.04	19.0

Table 16: Measured ^{41}Ca values from the irradiated barite concrete samples at CologneAMS (x1 and x2) and the diluted samples.

Sample-ID	$^{41}Ca/^{40}Ca$	Error ($^{41}Ca/^{40}Ca$)	rel. Error [%]	Ionic current [nA]	Atoms counted (^{41}Ca)
CaBlank1	4.71E-13	7.17E-14	15.22	3.37E-08	45
CaBlank2	2.08E-13	4.47E-14	21.54	3.74E-08	22
BB01x1	1.69E-11	8.57E-13	5.08	1.18E-08	613
BB01x2	1.67E-11	8.63E-13	5.18	1.12E-08	578
BB02x1	5.42E-11	2.05E-12	3.78	1.25E-08	2097
BB02x2	5.35E-11	1.99E-12	3.73	1.38E-08	2287
BB02_1	3.16E-12	2.04E-13	6.46	3.19E-08	311
BB03x1	1.64E-10	5.46E-12	3.33	1.28E-08	6504
BB03x2	1.65E-10	5.54E-12	3.35	1.15E-08	5876
BB03_1	5.77E-11	1.99E-12	3.45	2.40E-08	4281
BB03_2	1.57E-11	6.18E-13	3.93	3.48E-08	1692
BB04x1	5.50E-10	1.74E-11	3.17	1.14E-08	19280
BB04x2	5.52E-10	1.75E-11	3.17	1.17E-08	19900
BB04x3	3.82E-11	1.53E-12	4.00	1.32E-08	1553
BB04_1	7.52E-12	3.65E-13	4.86	3.06E-08	711
BB04_2	2.51E-12	1.83E-13	7.27	3.24E-08	231
BB05x1	1.61E-09	5.03E-11	3.12	1.07E-08	48904
BB05x2	1.65E-09	5.14E-11	3.12	1.19E-08	55321
BB05_1	4.65E-10	1.46E-11	3.14	2.38E-08	31266
BB05_2	1.10E-10	3.57E-12	3.26	2.99E-08	9276
BB05_3	3.69E-11	1.28E-12	3.48	3.71E-08	3869
BB05_4	7.63E-12	3.58E-13	4.69	3.71E-08	801

Table 17: Measured ^{14}C values from the irradiated barite concrete samples at CologneAMS.

Sample-ID	Type	He^{4+} [muA]	^{14}C/^{12}C	F14C	Error	Rel. Error [%]	Counts
Blank	blank	11.87	2.54E-14	0.0218	0.0021	9.791	366
Blank	blank	10.30	3.05E-14	0.0261	0.0024	9.376	294
B01_1	u	9.55	4.32E-12	3.6429	0.2015	5.532	949
B01_2	u	10.41	3.90E-12	3.3050	0.1488	4.503	47642
B02_1	u	10.85	6.29E-12	5.3314	0.2403	4.507	40712
B02_2	u	10.79	6.08E-12	5.1851	0.2332	4.498	61716
B03_1	u	9.52	9.46E-12	8.0086	0.3608	4.505	43342
B03_2	u	11.06	9.41E-12	8.0163	0.3607	4.499	57198
B04_1	u	10.46	4.56E-11	38.5552	1.7337	4.497	65237
B04_2	u	7.19	4.29E-11	36.8170	1.6576	4.502	49292
B05_1	u	10.72	1.73E-10	147.0343	6.5964	4.486	166885
B05_2	u	10.08	2.01E-10	171.2540	7.7135	4.504	45419